Article

Developmental Cell

Zebrafish Regulatory T Cells Mediate Organ-Specific Regenerative Programs

Highlights

- T_{reg} cells are required for spinal cord, heart, and retina regeneration in zebrafish
- T_{reg} cells promote regeneration by producing tissue-specific growth factors
- Pro-regenerative T_{reg} cell activity is distinct from immunosuppressive functions
- Zebrafish Foxp3a is essential for the production of tissue-specific growth factors

Authors

Subhra P. Hui, Delicia Z. Sheng, Kotaro Sugimoto, Alvaro Gonzalez-Rajal, Shinichi Nakagawa, Daniel Hesselson, Kazu Kikuchi

Correspondence

k.kikuchi@victorchang.edu.au

In Brief

Hui et al. show that zebrafish regulatory T (zT_{reg}) cells infiltrate damaged spinal cords, hearts, and retinas and are essential for robust regeneration. Infiltrating zT_{reg} cells produce tissue-specific pro-regenerative factors that stimulate tissue-resident precursor cell proliferation, revealing new cellular targets for increasing regenerative capacity in poorly regenerating species.

Hui et al., 2017, Developmental Cell *43*, 659–672
December 18, 2017
https://doi.org/10.1016/j.devcel.2017.11.010

CellPress

Developmental Cell
Article

Zebrafish Regulatory T Cells Mediate Organ-Specific Regenerative Programs

Subhra P. Hui,[1] Delicia Z. Sheng,[1,5] Kotaro Sugimoto,[1,5] Alvaro Gonzalez-Rajal,[1] Shinichi Nakagawa,[2,3] Daniel Hesselson,[3,4] and Kazu Kikuchi[1,4,6,*]

[1]Developmental and Stem Cell Biology Division, Victor Chang Cardiac Research Institute, Darlinghurst, NSW 2010, Australia
[2]Evolution and Ecology Research Centre, School of Biological, Earth and Environmental Sciences, University of New South Wales, Kensington, NSW 2052, Australia
[3]Diabetes and Metabolism Division, Garvan Institute of Medical Research, Darlinghurst, NSW 2010, Australia
[4]St. Vincent's Clinical School, University of New South Wales, Kensington, NSW 2052, Australia
[5]These authors contributed equally
[6]Lead Contact
*Correspondence: k.kikuchi@victorchang.edu.au
https://doi.org/10.1016/j.devcel.2017.11.010

SUMMARY

The attenuation of ancestral pro-regenerative pathways may explain why humans do not efficiently regenerate damaged organs. Vertebrate lineages that exhibit robust regeneration, including the teleost zebrafish, provide insights into the maintenance of adult regenerative capacity. Using established models of spinal cord, heart, and retina regeneration, we discovered that zebrafish T_{reg}-like (zT_{reg}) cells rapidly homed to damaged organs. Conditional ablation of zT_{reg} cells blocked organ regeneration by impairing precursor cell proliferation. In addition to modulating inflammation, infiltrating zT_{reg} cells stimulated regeneration through interleukin-10-independent secretion of organ-specific regenerative factors (Ntf3: spinal cord; Nrg1: heart; Igf1: retina). Recombinant regeneration factors rescued the regeneration defects associated with zT_{reg} cell depletion, whereas Foxp3a-deficient zT_{reg} cells infiltrated damaged organs but failed to express regenerative factors. Our data delineate organ-specific roles for T_{reg} cells in maintaining pro-regenerative capacity that could potentially be harnessed for diverse regenerative therapies.

INTRODUCTION

Most differentiated mammalian tissues, including the spinal cord, heart, and retina, show minimal regenerative reserve. In contrast, damage to these same zebrafish tissues induces spectacular regenerative responses, providing a model to identify pro-regenerative signals and pathways that may have been lost in the mammalian lineage. The proliferation of tissue-resident precursor cells, such as neural stem cells (ependymo-radial glial cells) in the spinal cord (Goldshmit et al., 2012; Reimer et al., 2008), Müller glia in the retina (Fausett and Goldman, 2006; Thummel et al., 2008), and cardiomyocytes in the heart (Jopling et al., 2010; Kikuchi et al., 2010), is essential for functional regenerative outcomes. The regenerative response involves localized inflammation and complex interactions between tissue-resident and systemically recruited immune cells with damaged parenchymal cells. Although inflammatory signals have been implicated in the initiation and completion of wound healing and regeneration (Fang et al., 2013; Hasegawa et al., 2017; Kyritsis et al., 2012; Lai et al., 2017), potential roles for immune cells in regulating precursor cell expansion remain largely unexplored.

Robust regenerative capacity is more prevalent in phyla that lack a sophisticated adaptive immune system, leading to the suggestion that adaptive immunity evolved at the expense of robust regenerative capacity (Mescher and Neff, 2005). Consistent with this hypothesis, T cells, key cellular effectors of the adaptive immune response, differentiate at the onset of the regeneration-refractory period during *Xenopus* development (Fukazawa et al., 2009). However, *Xenopus* tadpoles regain regenerative capacity at later developmental stages (Fukazawa et al., 2009), suggesting that efficient regeneration remains possible in the context of adaptive immunity (Aurora and Olson, 2014). Similarly, regenerative adult zebrafish possess a conserved adaptive immune system with fully functional T cells (Trede et al., 2004). Despite extensive functional analyses of innate immune cells (e.g., neutrophils and macrophages) in tissue regeneration (de Preux Charles et al., 2016; Hasegawa et al., 2017; Huang et al., 2013; Lai et al., 2017; Li et al., 2012; Petrie et al., 2015), the role of T cells in highly regenerative animals remains unclear.

A specialized T cell subtype, the regulatory T (T_{reg}) cell, maintains tolerance to self-antigens and restrains excessive inflammatory responses to infection and tissue damage (Josefowicz et al., 2012; Sakaguchi et al., 2010). In certain mouse tissues (e.g., skeletal muscle, lung epithelium, and skin), infiltrating T_{reg} cells modulate tissue-resident stem cell proliferation and differentiation after injury (Ali et al., 2017; Arpaia et al., 2015; Burzyn et al., 2013; Castiglioni et al., 2015; Nosbaum et al., 2016). Recently, an analogous homeostatic role was identified for T_{reg} cells in the maintenance of nerve myelination (Dombrowski et al., 2017). In contrast, mouse T_{reg} cells also infiltrate minimally regenerative tissues (e.g., heart or CNS), but are not sufficient to promote regeneration despite exerting a profound immunomodulatory effect (Raposo et al., 2014; Weirather

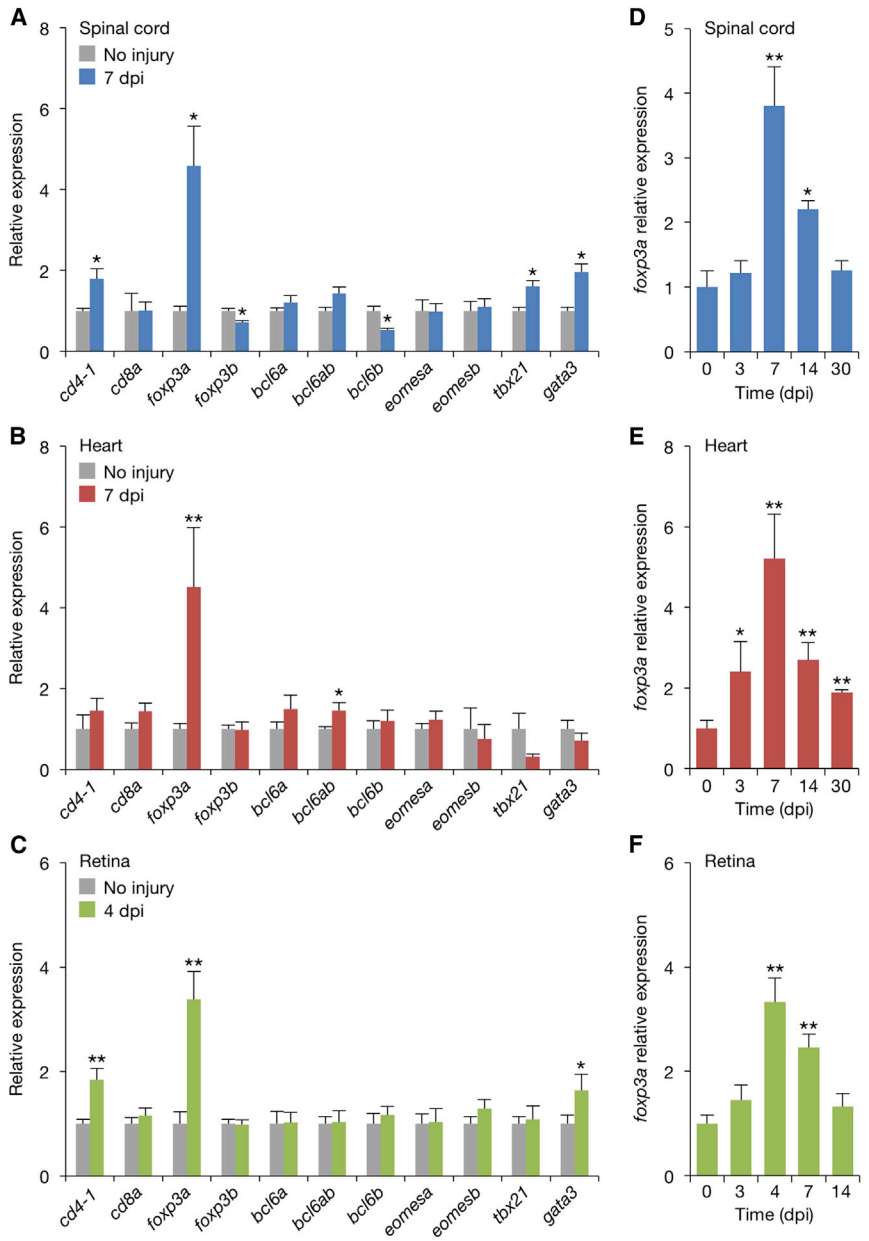

Figure 1. Expression of T Cell Markers in Regenerating Zebrafish Tissues

(A–C) qRT-PCR analysis of T cell markers (mean ± SEM n = 5).

(D–F) Time course of *foxp3a* expression (mean ± SEM, n = 5).

Gene expression is shown relative to the levels in uninjured controls. Uninjured tissues are indicated as 0 dpi in (D) to (F). *p < 0.05, **p < 0.01, Mann-Whitney U test. dpi, days post injury.

et al., 2014). It remains an important goal to determine whether T_{reg} cells retained limited regenerative functions in certain mammalian tissues or lost global pro-regenerative activity in non-regenerative tissues due to competing selective pressures.

Mammalian T_{reg} cell differentiation is controlled by the Forkhead box P3 (FOXP3) transcription factor (Brunkow et al., 2001; Fontenot et al., 2003; Hori et al., 2003). FOXP3 orthologs have been identified in amphibian and fish genomes (Andersen et al., 2012; Mitra et al., 2010; Quintana et al., 2010), and recent studies have demonstrated a conserved immunomodulatory role for FOXP3 in zebrafish (Quintana et al., 2010; Sugimoto et al., 2017). FOXP3 expression was upregulated after the developmental refractory period in *Xenopus* tadpoles (Fukazawa et al., 2009). However, a functional role for FOXP3-expressing cells has not been demonstrated in non-mammalian vertebrate regeneration.

Here, we investigated the role of zebrafish FOXP3 in the regeneration of distinct organ systems. Zebrafish FOXP3-expressing T cells, termed zT_{reg} cells, rapidly infiltrated damaged spinal cords, retinas, and hearts, and stimulated regenerative precursor cell proliferation by producing organ-specific pro-regenerative factors. zT_{reg}-derived regeneration factors were necessary and sufficient to support robust regenerative responses, which were functionally distinct from canonical immunomodulatory roles. Our findings demonstrate tissue-specific roles for T_{reg} cells in organ regeneration and provide a rationale for new T_{reg} cell-mediated regenerative therapies in humans.

RESULTS

A Zebrafish *FOXP3* Ortholog Is Induced during Organ Regeneration

We analyzed a panel of T cell markers in zebrafish spinal cord, heart, and retina regeneration. Remarkably, *forkhead box P3a* (*foxp3a*), which encodes a zebrafish ortholog of the mammalian master regulator of T_{reg} cell development and function, was the most prominently upregulated gene in distinct regenerative contexts (Figures 1A–1C). The expression of *foxp3a* transiently peaked at 7 days post injury (dpi) in damaged spinal cords and hearts (Figures 1D and 1E) and at 4 dpi in damaged retinas (Figure 1F), corresponding to the maximal organ-specific regenerative responses in these organs (Fausett and Goldman, 2006; Poss et al., 2002; Reimer et al., 2008).

A T Cell Subpopulation Defined by *foxp3a* Expression

Zebrafish *foxp3a* has been implicated in the regulation of inflammatory responses (Quintana et al., 2010; Sugimoto et al., 2017). However, the development and function of zebrafish *foxp3a*$^{+}$ cells has not been thoroughly investigated. Thus, we generated *TgBAC*(*foxp3a*:*TagRFP*)^{vcc3} (*foxp3a*:*RFP*), in which fluorescent TagRFP is under the control of a bacterial artificial chromosome (BAC) containing *foxp3a* regulatory elements. A small number of

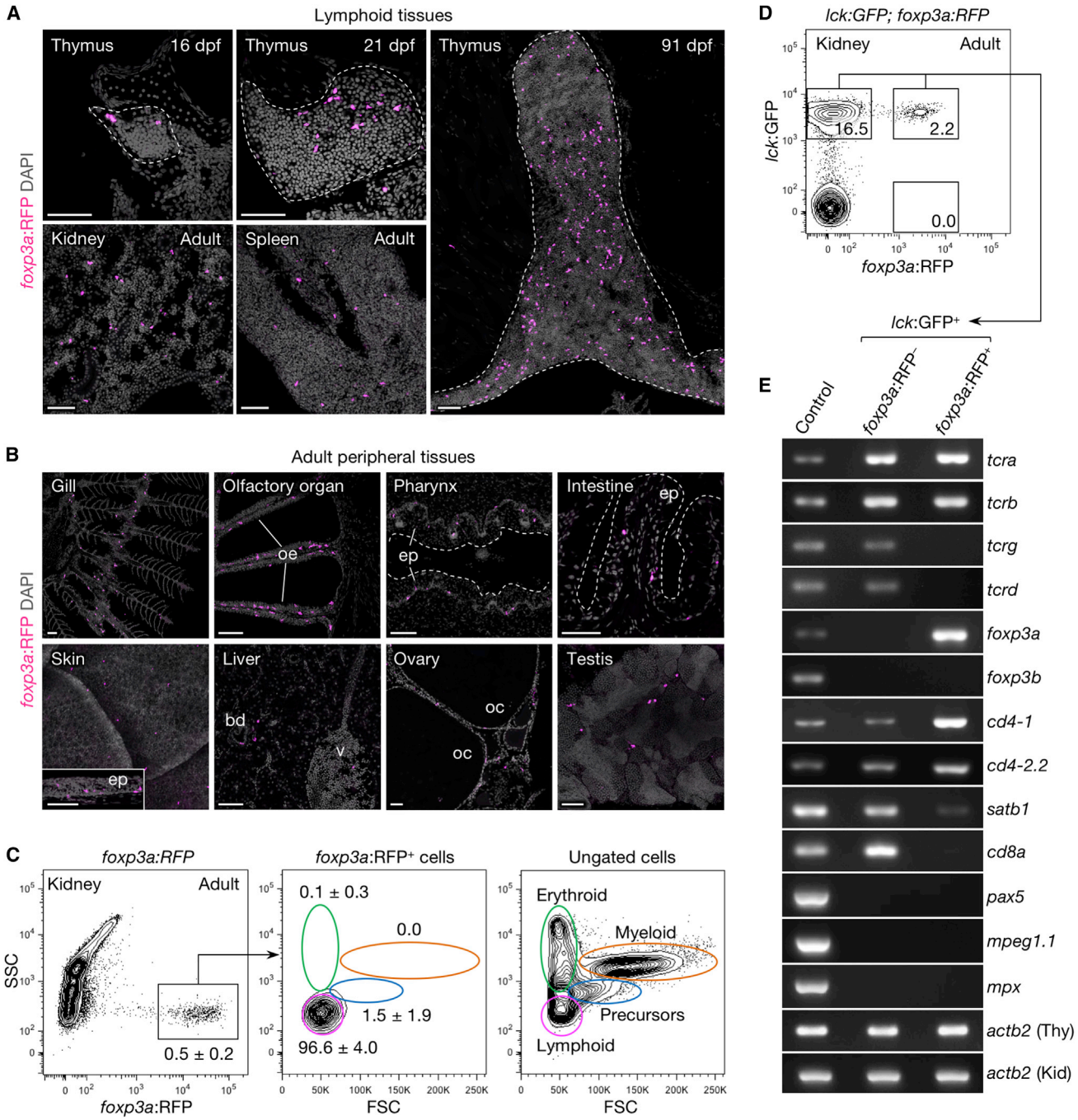

Figure 2. Distribution and Characterization of Zebrafish *foxp3a*$^{+}$ Cells

(A and B) *foxp3a*:RFP^{+} cells in lymphoid (A) and adult peripheral tissues (B).

(C and D) FACS analysis of total kidney cells from adult *foxp3a:RFP* (C) and *lck:GFP;foxp3a:RFP* fish (D). The percentage of cells in each gate are indicated in the plots (C; mean ± SD, n = 5). The lymphoid gate from (C) is shown in (D).

(E) Semi-qRT-PCR analysis of purified *lck*:GFP^{+}*foxp3a*:RFP^{-} (upper-left gate in D) and *lck*:GFP^{+}*foxp3a*:RFP^{+} cells (upper-right gate in D). Thymus (Thy) and kidney (Kid) cell suspension was used as control for T cell genes and non-T cell genes.

bd, bile duct; ep, epithelium; oe, olfactory epithelium; oc, oocyte; v, vein; FSC, forward scatter; SSC, side scatter. Scale bars, 50 μm.

foxp3a:RFP^{+} cells were detected in the thymus by 16 days post fertilization (dpf), and accumulated further during development (Figure 2A). In the adult, *foxp3a*:RFP^{+} cells were most abundant in the kidney, which has both diuretic and hematopoietic functions in zebrafish ($1.7 \pm 0.1 \times 10^{4}$ cells per organ, n = 9; Figure 2A), with fewer cells in the thymus ($5.9 \pm 1.4 \times 10^{3}$ cells per organ, n = 6; Figure 2A) and the spleen ($3.0 \pm 0.3 \times 10^{2}$ cells per organ, n = 8; Figure 2A). The *foxp3a*:RFP^{+} cells were

frequently detected in tissues that are exposed to external stimuli, such as the gills, the olfactory epithelium, the skin epidermis, and the mucosal surfaces of the pharynx and intestine (Figure 2B). The *foxp3a*:RFP$^+$ cells were also observed in the liver and reproductive organs (Figure 2B), but were rarely detected in other internal organs.

By flow cytometry, *foxp3a*:RFP$^+$ cells represented 0.5% of the total cells in the adult kidney (Figure 2C) and were exclusively confined to the lymphoid gate (Figure 2C, magenta gate) (Traver et al., 2003). To determine whether *foxp3a* expression was lineage restricted, we generated *foxp3a*:*RFP*;*TgBAC*(*lck*:*GFP*)^{vcc4} (*lck*:*GFP*) (Sugimoto et al., 2017) double transgenics in which GFP is under the control of a BAC containing T cell-specific *lck* regulatory elements (Langenau et al., 2004). All *foxp3a*:RFP$^+$ kidney cells co-expressed *lck*:GFP (Figure 2D, upper-right gate). The *foxp3a*:RFP$^+$ cells comprised 12% of the total *lck*:GFP$^+$ cell population (Figure 2D), which was approximately 3-fold greater than the proportion observed in murine peripheral lymphoid organs (3.9% of TCRβ$^+$ cells) (Fontenot et al., 2005).

To further define the transcriptional program of zebrafish Foxp3a$^+$ cells, we used fluorescence-activated cell sorting (FACS) to purify *lck*:GFP$^+$*foxp3a*$^+$ cells (Figure 2D, upper-right gate), which were compared with *lck*:GFP$^+$*foxp3a*$^-$ cells (Figure 2D, upper-left gate) (Figure 2E). Similar to mouse T$_{reg}$ cells that are derived from the αβ T cell lineage (Sakaguchi, 2004), zebrafish *foxp3a*$^+$ T cells expressed T cell receptor (TCR) α (*tcra*) and β (*tcrb*) but not TCR γ (*tcrg*) or δ (*tcrd*) (Figure 2E). Markers of non-T cell lymphoid lineages such as *pax5* (B cells), *mpeg1.1* (macrophages), and *mpx* (neutrophils) were not detected (Figure 2E). In contrast to *foxp3a*, the expression of the *foxp3b* paralog was not detected in *lck*:GFP$^+$ cells (Figure 2E), suggesting that *foxp3a* is the functional FOXP3 ortholog in adult zebrafish T cells. Next, we analyzed additional zebrafish T cell markers (Dee et al., 2016). Similar to mouse T$_{reg}$ cells, the *foxp3a*$^+$ cells exhibited enrichment of the *CD4* paralogs (*cd4-1* and *cd4-2.2*), accompanied by depletion of *CD8* (*cd8a*) compared with *foxp3a*$^-$ cells (Figure 2E). Furthermore, *satb1*, a negatively regulated target of Foxp3 in mouse and human T$_{reg}$ cells (Beyer et al., 2011), was downregulated in *foxp3a*$^+$ cells (Figure 2E). Together, these data indicate that zebrafish possess T cell lineage with a conserved T$_{reg}$ cell expression profile, which we term zT$_{reg}$ cells.

zT$_{reg}$ Cells Infiltrate Injury Sites and Persist during Regeneration

While zT$_{reg}$ cells were largely absent in uninjured organs, zT$_{reg}$ cells infiltrated damaged organs between 3 and 7 dpi and remained until regeneration was complete (Figure 3A). zT$_{reg}$ cell infiltration peaked between 4 dpi (retina) and 7 dpi (spinal cord and heart) (Figure 3B), matching the time points that showed the highest *foxp3a* expression (Figures 1D–1F).

Concomitant with the emergence of zT$_{reg}$ cells at injury sites, there was a dramatic increase in systemically circulating *foxp3a*:RFP$^+$ cells in peripheral blood (Figures 3C and 3D), suggesting that zT$_{reg}$ cells were mobilized in response to a cue derived from damaged tissues. We labeled proliferative cells with ethynyl-2′-deoxyuridine (EdU) after injury and detected EdU$^+$*foxp3a*:RFP$^+$ cells (Figure 3E, arrows), indicating that infiltrating zT$_{reg}$ cells proliferated during the regenerative response. Nrp1 and Helios are expressed at higher levels in mouse thymus-derived T$_{reg}$ cells compared with peripherally derived T$_{reg}$ cells (Thornton et al., 2010; Weiss et al., 2012; Yadav et al., 2012). zT$_{reg}$ cells isolated from damaged organs exhibited robust expression of *nrp1a* and *helios* compared with control zT$_{reg}$ cells isolated from undamaged kidneys (Figure 3F). Together, these data suggest that organ damage stimulates the mobilization and expansion of mature zT$_{reg}$ cells, as opposed to the differentiation of zT$_{reg}$ cells at the injury site.

zT$_{reg}$ Cells Are Required for Organ Regeneration

To investigate whether zT$_{reg}$ cells are required for efficient regeneration, we generated *TgBAC*(*foxp3a*:*TagCFP-NTR*)^{vcc5} (*foxp3a*:*NTR*), which labels zT$_{reg}$ cells with TagCFP and permits lineage-specific ablation by nitroreductase (NTR)-mediated conversion of the pro-drug metronidazole (Mtz) to a cytotoxic agent (Curado et al., 2007; Pisharath et al., 2007). We confirmed that *foxp3a*:NTR$^+$ cells were efficiently depleted in damaged tissues after Mtz administration (Figures S1A–S1D) but rapidly recovered after Mtz washout (Figures S1B–S1D), suggesting that zT$_{reg}$ cells were continuously recruited to the injury sites. To ensure continuous zT$_{reg}$ cell depletion during regeneration, we established an optimized Mtz treatment regimen (Figure S1E), which achieved similar *foxp3a* expression levels in damaged tissues as compared with uninjured control tissue (Figures S1F–S1H), without inducing a systemic inflammatory cytokine response (Figure S1I).

Using this regimen, we depleted zT$_{reg}$ cells after spinal cord transection. To control for transgene expression and potential Mtz toxicity, the control groups comprised vehicle (Veh)-treated *foxp3a*:*NTR* fish and Mtz-treated wild-type (WT) fish. Both control groups were indistinguishable; the vast majority of damaged spinal cords regenerated with no gap observed at the transected site by 30 dpi (Figure 4A, Normal in 4C). In contrast, zT$_{reg}$ cell-depleted fish exhibited disorganized axonal sprouts emanating from the rostral and caudal stumps at 30 dpi (Figure 4A, Severe in 4C). Approximately one-third of zT$_{reg}$ cell-depleted fish lacked any regrowth from the rostral and caudal stumps (Figure 4C, Very severe). The rostral and caudal stumps remained disconnected in zT$_{reg}$ cell-depleted spinal cords at 30 dpi, which was verified by retrograde tracing of axonal projections (Figure 4B). Functional recovery, assessed by locomotor activity, was also severely impaired by zT$_{reg}$ cell depletion at 30 dpi, a time point by which Mtz-treated WT control fish had regained pre-injury swimming performance (Figures 4D and 4E).

We next assessed the role of zT$_{reg}$ cells during cardiac and retinal regeneration. The zebrafish cardiac ventricle was damaged using a cryoinjury model (Chablais et al., 2011; González-Rosa et al., 2011; Schnabel et al., 2011). The majority of control hearts vigorously regenerated a thick muscle wall that encapsulated the residual scar tissue by 45 dpi (Figure 4F, Mild in 4G). In contrast, zT$_{reg}$ cell-depleted hearts formed a thinner myocardial wall with striking deposition of fibrin and a persisting collagenous scar (Figure 4F, Severe in 4G; Quantification in 4H). Similarly, we examined retinal regeneration using a needle-poke injury model (Senut et al., 2004). While the retina regenerated with a normal (Figure 4I, Normal in 4J) or slightly distorted (Moderate in Figure 4J) layer structure in the control

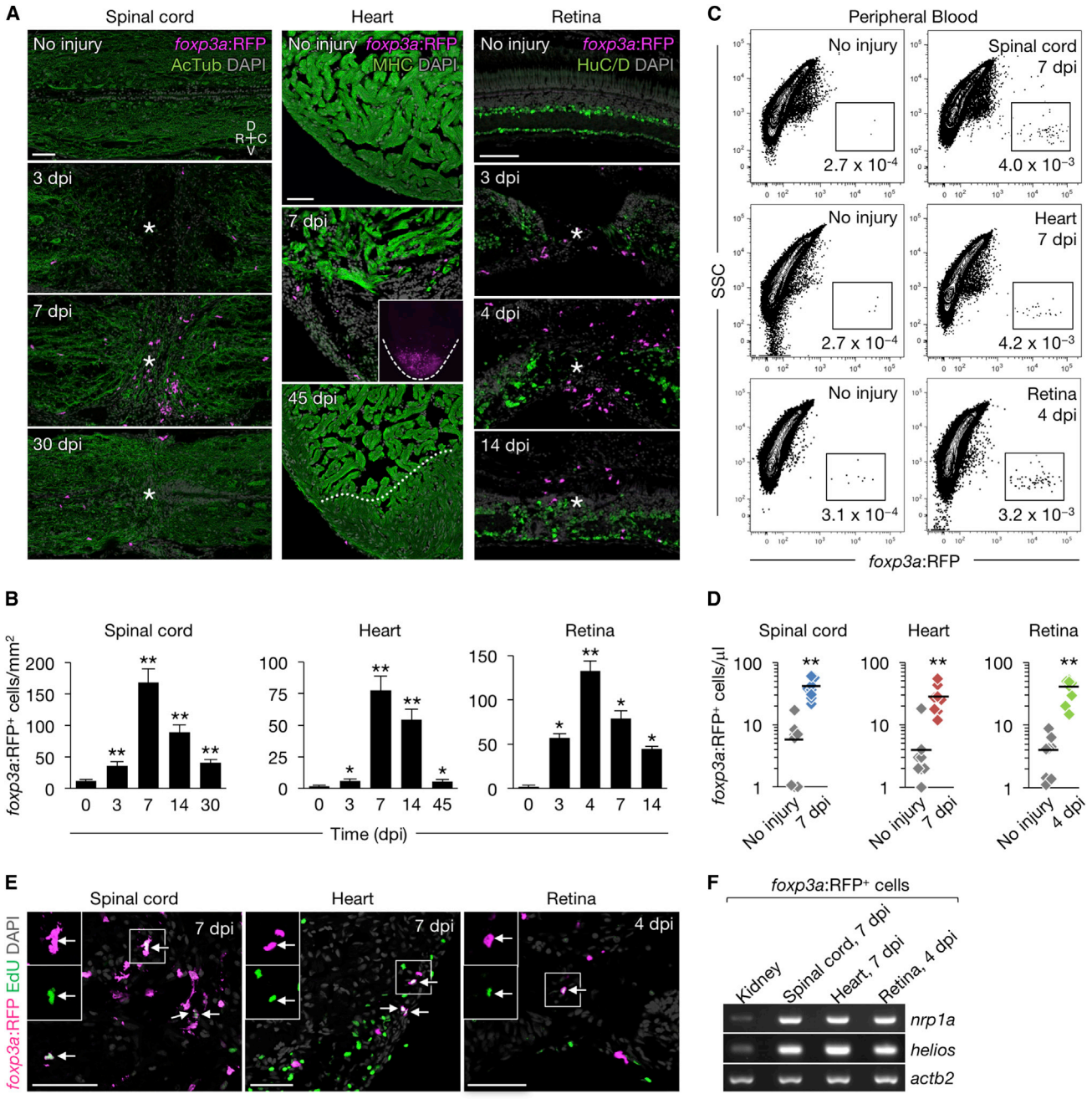

Figure 3. Zebrafish *foxp3a*$^{+}$ Cells Infiltrate Regenerating Tissues

(A) Sections of injured and uninjured *foxp3a:RFP* tissues. Immunofluorescence for acetylated Tubulin (AcTub), myosin heavy chain (MHC), and HuC/D marks nerves, cardiac muscle, and neuronal cells, respectively. Asterisks indicate injury epicenter. The dashed line in the inset outlines the ventricle, and the dotted line indicates the border of the regenerated muscle.

(B) Quantification of *foxp3a*:RFP^{+} cells in A (mean ± SEM, n = 5–8). Uninjured tissues are indicated as 0 dpi.

(C) FACS analysis of peripheral blood *foxp3a*:RFP^{+} cells. The percentages of cells in each fraction are shown in the plot.

(D) Quantification of *foxp3a*:RFP^{+} cells in (C) (n = 8).

(E) EdU labeling of injured *foxp3a:RFP* tissues. EdU was injected intraperitoneally at 4, 5, and 6 days after spinal cord and heart injury, or 3 days after retina injury. Arrows point to co-labeled cells. Insets: single-channel images of the marked regions.

(F) Semi-qRT-PCR analysis of purified *foxp3a*:RFP^{+} cells.

C, caudal; D, dorsal; R, rostral; V, ventral. Confocal projections of z stacks are shown in (A) and (E). *$p < 0.01$, **$p < 0.01$, Mann-Whitney U test. Scale bars, 50 μm.

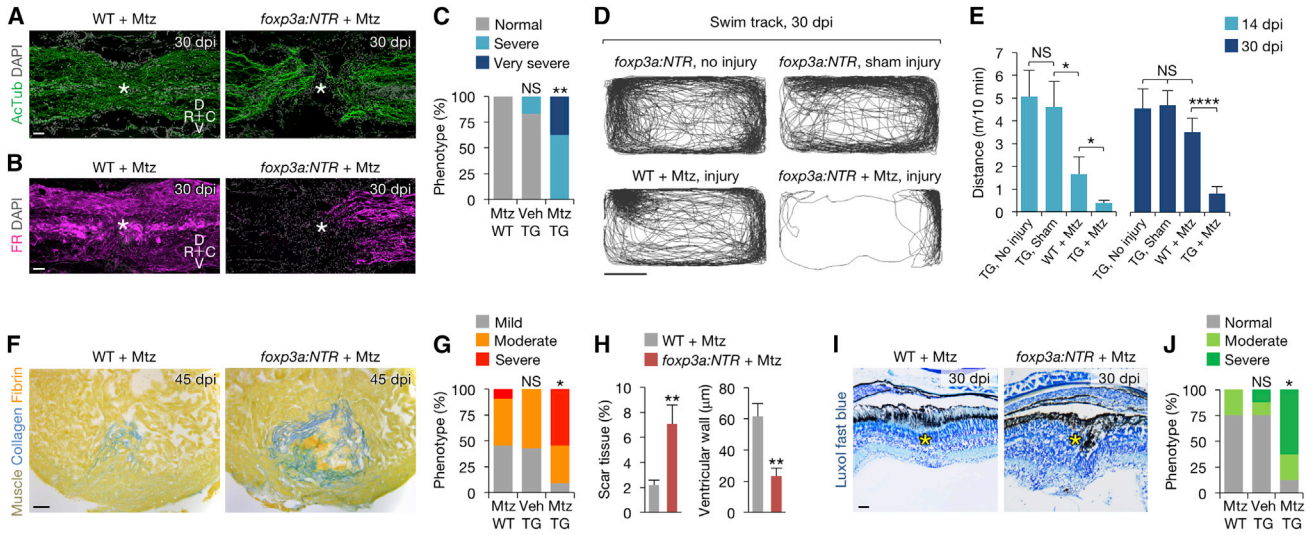

Figure 4. zT_{reg} Cells Are Required for Organ Regeneration

(A) Spinal cord sections from control (left) and zT_{reg} cell-ablated fish (right).

(B) Retrograde tracing of axonal projections using Fluoro-Ruby (FR). Regenerating axons spanned the transection injury in control fish (left; 6/6) but not zT_{reg} cell-depleted fish (right; 1/6; $p < 0.05$).

(C) Quantification of regeneration in (A) (n = 6–8).

(D) Swim tracking of individual animals after spinal cord injury.

(E) Quantification of total distance moved in (D) (mean ± SEM, n = 8–14).

(F) Picro-Mallory staining of heart sections from control (left) and zT_{reg} cell-ablated fish (right).

(G) Quantification of regeneration in (F) (n = 7–10).

(H) Quantification of scar tissue size (left) and myocardial wall thickness (right) in (F) (mean ± SEM, n = 10).

(I) Luxol fast blue staining of retina sections from control (left) and zT_{reg} cell-ablated fish (right).

(J) Quantification of regeneration in (I) (n = 8).

Asterisks indicate injury epicenter. Mtz, metronidazole; TG, *foxp3a:NTR*; Veh, vehicle; WT, wild-type. Confocal projections of z stacks are shown, except for the images in (F) and (I). NS, not significant; *$p < 0.05$, **$p < 0.01$, ****$p < 0.001$, Fisher's exact test (B, C, G, and J), unpaired two-tailed Student's t test with Welch correction (E), and Mann-Whitney U test (H). Scale bars, 50 μm (A, B, F, I) and 0.1 m (D). See also Figure S1.

fish, the layer structure remained severely disorganized in most zT_{reg} cell-depleted fish at 30 dpi (Figure 4I, Severe in 4J). Together, these results highlight a critical role for zT_{reg} cells in the regeneration of multiple zebrafish organs.

zT_{reg} Cells Promote Precursor Cell Proliferation in Damaged Organs

In zebrafish, CNS regeneration occurs via *de novo* neurogenesis following the activation and proliferation of neural progenitor cells (Barbosa et al., 2015; Kroehne et al., 2011; Reimer et al., 2008). In the damaged spinal cord of *TgBAC*(*foxp3a*:*EGFP*)^{vcc10} (*foxp3a*:*GFP*) fish, we observed *foxp3a*:GFP$^+$ cells near proliferating neural progenitor cells (Figure 5A, arrowheads) that were co-labeled with the neural progenitor marker Sox2 and proliferating cell nuclear antigen (PCNA) (Barbosa et al., 2015; Hui et al., 2015). Some *foxp3a*:GFP$^+$ cells were in direct contact with proliferating neural progenitor cells (Figure 5A, arrows). Moreover, *foxp3a*:GFP$^+$ cells (Figure 5B, arrows) remained near or in direct contact with newly differentiated HuC/D positive neurons (Figure 5B, arrowheads).

We next investigated whether zT_{reg} cells similarly stimulated precursor cell proliferation in regenerating hearts and retinas, which use distinct regenerative mechanisms. Following injury, the primary regenerative mechanism in the zebrafish heart involves the proliferation of spared cardiomyocytes (Jopling et al., 2010; Kikuchi et al., 2010). In contrast, retinal regeneration is mediated by injury-induced dedifferentiation of Müller glia, followed by the proliferation and differentiation of progenitors into all major retinal cell types (Fausett and Goldman, 2006; Thummel et al., 2008). In regenerating hearts at 7 dpi, zT_{reg} cells (Figure 5C, arrows) were near or in direct contact with proliferating cardiomyocytes (Figure 5C, arrowheads). Similarly, in regenerating retinas at 4 dpi, zT_{reg} cells (Figure 5D, arrows) were observed near proliferating Müller glia cells marked by PCNA and *Tg*(*gfap*:*EGFP*) (*gfap*:*GFP*) (Bernardos and Raymond, 2006) (Figure 5D, arrowheads). Together, these results suggest that zT_{reg} cells regulate precursor cell proliferation during diverse modes of organ regeneration.

To test whether zT_{reg} cells were required for regenerative precursor cell proliferation, we depleted zT_{reg} cells post injury. In the injured spinal cord, we observed significant reductions of proliferating Sox2$^+$ neural progenitors at 7 dpi (Figures 5E and 5I) and recently proliferated HuC/D$^+$ newborn neurons at 14 dpi after zT_{reg} cell depletion (Figures 5F and 5J). Similarly, zT_{reg} cell depletion significantly reduced Mef2$^+$ cardiomyocyte proliferation in the damaged heart (Figures 5G and 5K), and *gfap*:GFP$^+$ Müller glia proliferation in the damaged retina (Figures 5H and 5L). Pro-survival gene expression (Figures S2A–S2C) and caspase-3 activation

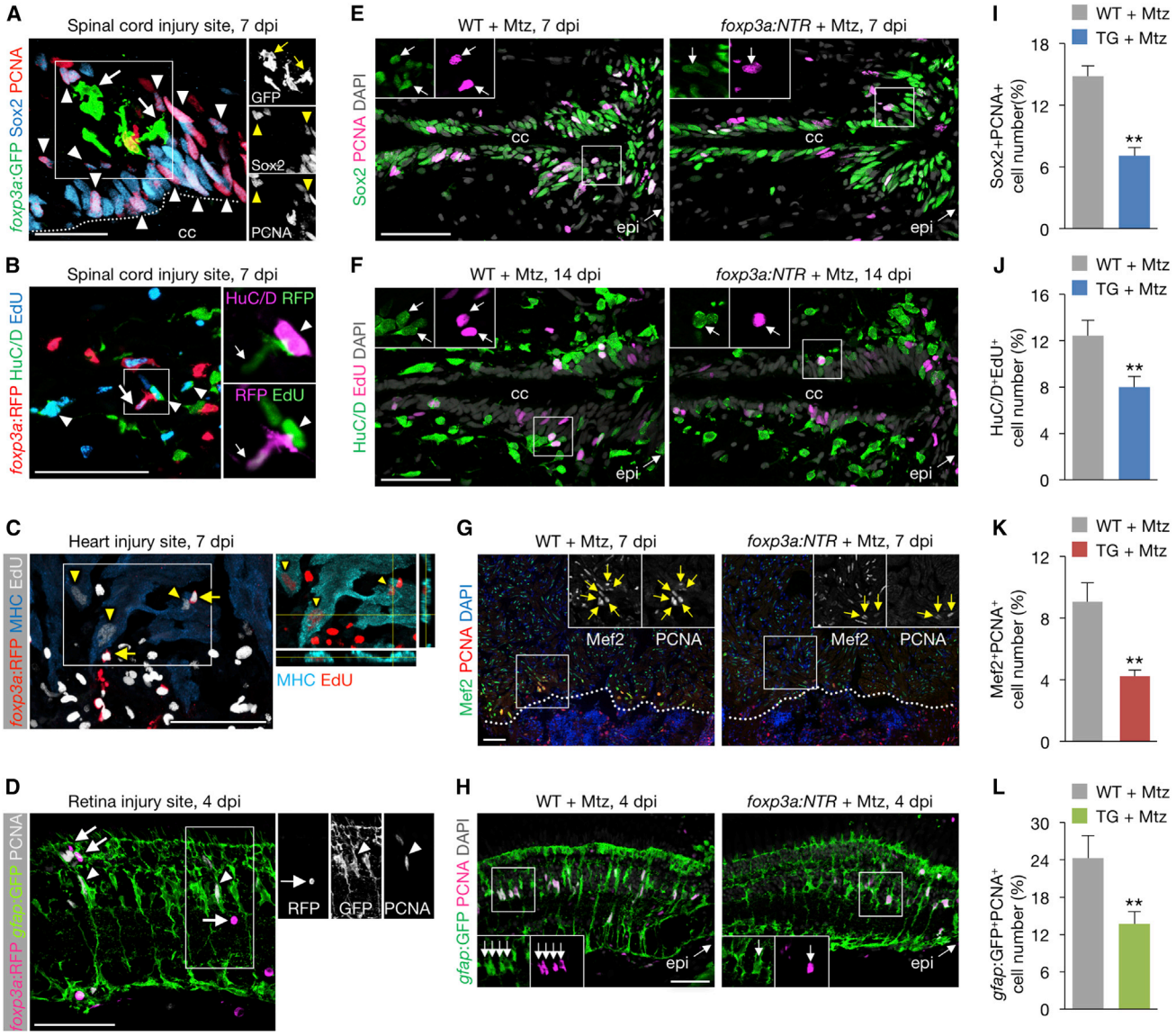

Figure 5. zT_{reg} Cells Promote Regenerative Precursor Cell Proliferation

(A and B) zT_{reg} cells (arrows) interacting with proliferating neural progenitor cells (A; arrowheads point to $Sox2^+PCNA^+$) and newly differentiated neurons (B; arrowheads point to HuC/D^+EdU^+). Right panels show single-channel confocal sections of the demarcated regions. The dotted line marks the border of the central canal (cc).

(C) zT_{reg} cells (arrows) interacting with proliferating cardiomyocytes (arrowheads point to MHC^+EdU^+). Image on the right shows the xz and yz planes of the demarcated region.

(D) zT_{reg} cells (arrows) interacting with proliferating Müller glia (arrowheads point to *gfap*:GFP^+PCNA^+). Right panels show single-channel confocal sections of the demarcated region.

(E–H) Proliferation of neural progenitor cells (E), newly differentiated neurons (F), cardiomyocytes (G), and Müller glia (H). Insets show single-channel confocal slices (E, F, and H) or epifluorescent images (G) of the demarcated regions. Arrows mark co-labeled cells. Dotted lines indicate the wound border. epi, injury epicenter.

(I–L) Quantification of (E), (F), (G), and (H), respectively (mean ± SEM, n = 6–7).

Confocal projections of z stacks are shown, except for the epifluorescent images in (G). **$p < 0.01$, Mann-Whitney U test. Scale bars, 50 μm.

were unaltered in the injured tissues after zT_{reg} cell depletion (Figures S2D–S2I), indicating that increasing cell survival was not a major regenerative mechanism. Instead, our results strongly support a model in which zT_{reg} cells enhance tissue regeneration by promoting the proliferation of organ-specific precursor cells.

zT_{reg} Cells Produce Tissue-Specific Regeneration Factors

To investigate the pro-regenerative mechanisms employed by zT_{reg} cells, we analyzed the expression of growth factors that were known to promote precursor cell proliferation during development and regeneration. Damaged zT_{reg} cell-depleted spinal

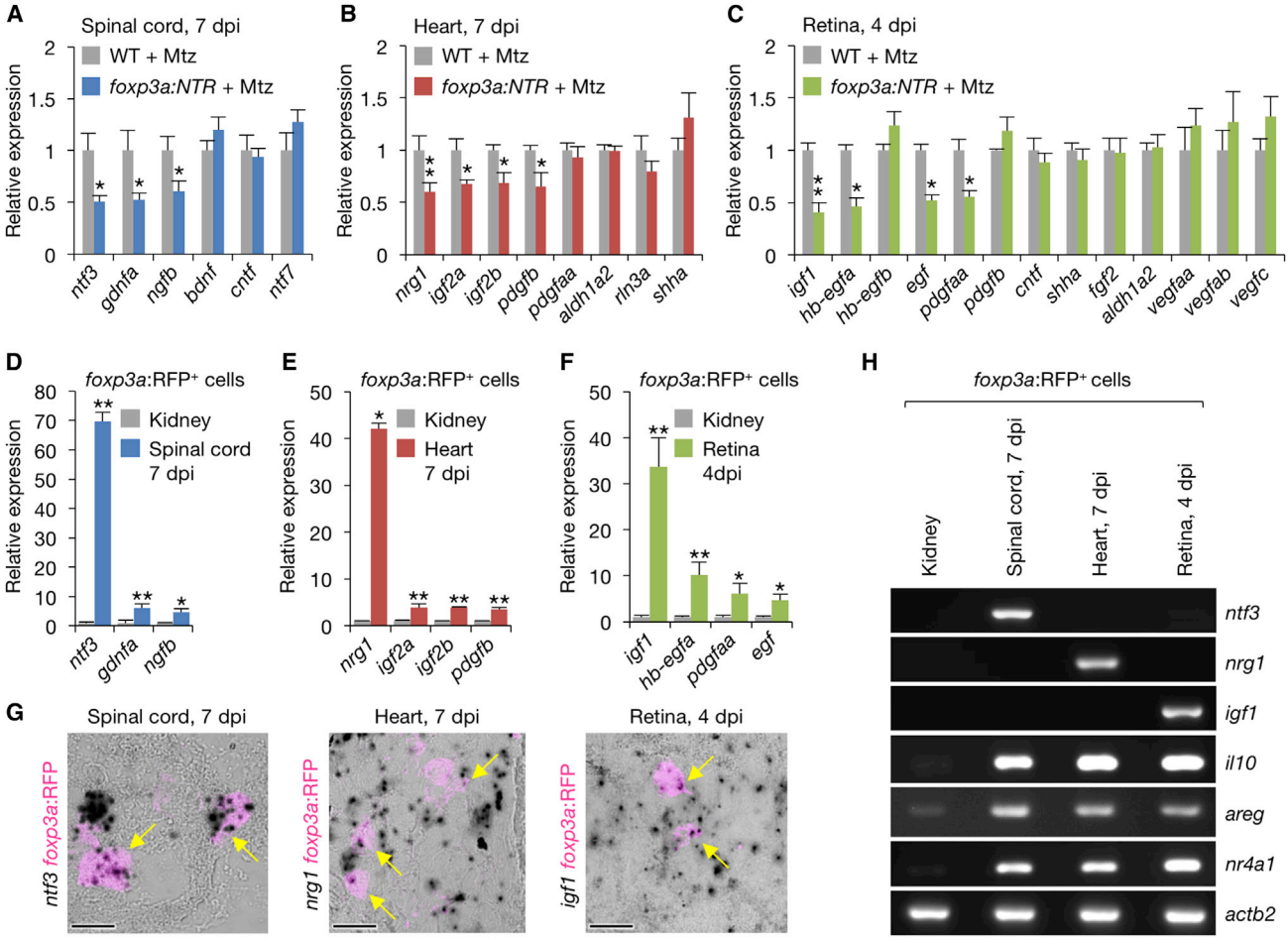

(legend on next page)

cords exhibited significantly reduced expression of the neurogenic factors *ntf3*, *gdnfa*, and *ngfb* at 7 dpi (Figure 6A). Similarly, the expression of cardiomyocyte mitogens *nrg1*, *igf2a*, *igf2b*, and *pdgfb* was reduced in 7-dpi zT_{reg} cell-depleted hearts (Figure 6B), and the expression of Müller glia growth factors *igf1*, *hb-egfa*, *egf*, and *pdgfaa* was reduced in 4-dpi zT_{reg} cell-depleted retinas (Figure 6C). To explore whether zT_{reg} cells were a significant source of precursor cell growth factors, we compared purified zT_{reg} cells from damaged tissues with kidney-derived zT_{reg} cells as an uninjured control population. All of the growth factor genes that were downregulated upon zT_{reg} cell depletion were significantly upregulated in zT_{reg} cells derived from the relevant damaged tissue compared with kidney-derived controls (Figures 6D–6F).

Among the induced growth factors, we identified a remarkable upregulation of a single factor in zT_{reg} cells from each damaged organ: neurotrophin 3 (*ntf3*/*nt3*) in the spinal cord (Figure 6D), neuregulin 1 (*nrg1*) in the heart (Figure 6E), and insulin-like growth factor 1 (*igf1*) in the retina (Figure 6F). To confirm that these factors were expressed by zT_{reg} cells, we performed high-resolution *in situ* hybridization and detected co-localization with *foxp3a*:RFP^+ cells at regenerating sites (Figure 6G, arrows). Strikingly, the predominant zT_{reg} cell-derived growth factor from each regenerating tissue was upregulated in a tissue-specific manner (Figure 6H). Thus, *ntf3* was expressed in spinal cord-derived zT_{reg} cells, but not in heart- and retina-derived zT_{reg} cells. Similarly, *nrg1* and *igf1* were exclusively expressed in heart- and retina-derived-zT_{reg} cells, respectively (Figure 6H). Moreover, these genes were not expressed in *foxp3a*$^-$ T cells that were purified from regenerating organs, highlighting the specificity of the zT_{reg} cell transcriptional response (Figure S3A).

In contrast to the tissue-specific expression of precursor cell growth factors, we detected a sharp induction of *nr4a1*, a T cell activation marker (Moran et al., 2011), in all injury-derived zT_{reg} cells (Figure 6H). This result, together with the observed proliferation of zT_{reg} cells at sites of injury (Figure 3E), suggests a model in which zT_{reg} cell activation occurs in the injured microenvironment during regeneration. Consistent with this model, mobilized zT_{reg} cells, isolated from peripheral blood after injury, did not exhibit upregulation of the major regeneration factors *ntf3*, *nrg1*, or *igf1* (Figure S3B). These results confirm that tissue injury per se does not induce global activation of zT_{reg} cells in remote tissues and suggests an important role for the regenerative microenvironment in programming the zT_{reg} cell response.

Injury-associated zT_{reg} cells also upregulated *amphiregulin* (*areg*) (Figures 6H and S3C), a factor required for murine T_{reg}-mediated lung and skeletal muscle repair (Arpaia et al., 2015; Burzyn et al., 2013). However, *areg* did not exhibit tissue specificity (Figure 6H) and was modestly induced (Figure S3C), presenting a stark contrast with the tissue-specific regulation and profound upregulation of the precursor cell growth factors (Figures 6D–6F and 6H). We conclude that injury-infiltrating zT_{reg} cells are activated and acquire a secretory phenotype unique to the tissue environment in which they reside, promoting tissue regeneration by enhancing the proliferation of tissue-specific precursor cells.

Recombinant zT_{reg}-Derived Factors Rescue Precursor Cell Proliferation in zT_{reg} Cell-Depleted Tissues

Ntf3 regulates neural stem cell maintenance (Delgado et al., 2014) and adult neurogenesis in rodent models (Shimazu et al., 2006). To address the functional relevance of zT_{reg}-derived Ntf3, we subjected *foxp3a*:*NTR* fish to spinal cord transection and Mtz treatment, followed by intraperitoneal injections of recombinant human NTF3 peptide or PBS (control) (Figures 6I and S4A). NTF3 treatment rescued the number of $Sox2^+PCNA^+$ cells at 7 dpi (Figures 6L and S4B) and HuC/D^+EdU^+ cells at 14 dpi (Figures S4C and S4F) to WT levels in the absence of zT_{reg} cells, indicating that NTF3 supplementation is sufficient to promote neurogenesis during spinal cord regeneration. In contrast, NTF3 did not induce neural progenitor proliferation (Figure 6L) or increase newborn neuron numbers (Figure S4F) in uninjured spinal cords. The expression of the Ntf3 receptors *ntrk3a* and *ntrk3b* were upregulated in purified *gfap*:GFP^+ ependymo-radial glial cells (Goldshmit et al., 2012) in response to spinal cord injury (Figure S4G), explaining the regeneration-specific effect of NTF3 supplementation (Figures 6L and S4F).

Analogous to the role of NTF3 in the spinal cord, NRG1 signaling promotes cardiomyocyte proliferation in zebrafish and mammalian hearts (Bersell et al., 2009; D'Uva et al., 2015; Gemberling et al., 2015; Polizzotti et al., 2015), while insulin/insulin-like growth factor 1 (IGF1) signaling induces regenerative responses in Müller glia cells (Fischer and Reh, 2002; Ritchey et al., 2012; Wan et al., 2014). Administration of human NRG1 (Figure 6J) or IGF1 peptides (Figure 6K) rescued cardiomyocyte (Figures 6M and S4D) or Müller glia proliferation (Figures 6N and S4E), respectively, in damaged zT_{reg} cell-depleted organs. Similar to NTF3, NRG1 and IGF1 administration did not induce cardiomyocyte or Müller glia proliferation in uninjured tissues (Figures 6M and 6N). Consistent with this observation, tissue damage strongly upregulated Nrg1 receptors (*erbb2*, *erbb4a*, and *erbb4b*) in sorted *Tg*(*cmlc2*:*EGFP*) (*cmlc2*:*GFP*) (Burns et al., 2005)-positive cardiomyocytes (Figure S4H), and Igf1 receptors (*igf1ra* and *igf1rb*) in *gfap*:GFP^+ Müller glia (Figure S4I). In contrast, Ntf3, Nrg1, or Igf1 receptors were not upregulated

Figure 6. zT_{reg} Cells Express Tissue-Specific Pro-regenerative Factors

(A–C) qRT-PCR analysis of growth factor expression in injured tissues (mean ± SEM, n = 6).

(D–F) qRT-PCR analysis of secreted factors in purified zT_{reg} cells (mean ± SD; *p < 0.05, **p < 0.01). Gene expression is shown relative to the levels in kidney-derived zT_{reg} cells.

(G) *In situ* hybridization using RNAscope and immunofluorescence against TagRFP in damaged *foxp3a*:*RFP* tissues. Arrows indicate zT_{reg} cells expressing mRNAs of *ntf3* (left), *nrg1*(middle), or *igf1*(right). Single confocal sections are shown.

(H) Semi-qRT-PCR analysis of zT_{reg} cells purified from injured tissues and uninjured kidneys.

(I–K) Experimental interventions involving NTF3 (I), NRG1 (J), or IGF1 (K) treatments. i.p., intraperitoneal injection; i.v., intravitreal injection.

(L–N) Quantification of proliferating neural progenitor cells (L), cardiomyocytes (M), and Müller glia (N) (n = 5–8). Representative images are shown in Figures S4B, S4F, and S4G.

*p < 0.05, **p < 0.01, Mann-Whitney U test (A–C and L–N) and Student's t test (D–F). Scale bars, 20 μm. See also Figure S4.

in zT_{reg} cells purified from injury sites (data not shown), suggesting that these pathways do not contribute to autocrine amplification of zT_{reg} cells.

zT_{reg} Cells Promote *il10*-Independent Stimulation of Precursor Cell Proliferation

In mice, T_{reg} cells promote CNS and cardiac repair by secreting immunosuppressive cytokines and regulating the balance between pro-inflammatory M1-like and regulatory M2-like macrophages (Kunis et al., 2015; Liesz et al., 2009; Raposo et al., 2014; Tang et al., 2012; Walsh et al., 2014; Weirather et al., 2014). Upon zT_{reg} cell ablation in zebrafish, pro-inflammatory genes were upregulated in damaged tissues (Figures S5A–S5C), but not in whole animal samples (Figures S5D–S5F), indicating that the inflammatory response is restricted to injury sites. In damaged tissues, zT_{reg} cell depletion also induced M1-biased changes in the macrophage markers *nos2b/inos2b* and *marco* (Figures S5G–S5I), suggesting a conserved role for zT_{reg} cells in restraining inflammation and regulating macrophage polarization during regeneration.

Interferon γ (IFNγ)-producing effector T cells play an important role in myocardial (Hofmann et al., 2012) and spinal cord repair in mice (Raposo et al., 2014). T_{reg} cells have been implicated in suppressing T cell responses in damaged hearts (Hofmann et al., 2012) and spinal cords (Raposo et al., 2014). We explored whether zT_{reg} cells modulate effector T cell responses in damaged tissues by isolating *TgBAC*(*lck*:*TagRFP*)^{vcc11} (*lck*:*RFP*)-positive T cells after zT_{reg} cell ablation. zT_{reg} cell depletion did not affect *lck*:RFP$^+$ T cell infiltration into damaged tissues (Figures S5J–S5O). Effector T cell markers, such as Th1 (*tbx21* and *ifng1-1*) and Th2 (*gata3* and *il4*) genes, were minimally altered in purified *lck*:RFP$^+$ cells from zT_{reg} cell-depleted damaged hearts (Figure S5Q) and retinas (Figure S5R). However, *tbx21* and the zebrafish IFNγ ortholog *ifng1-1* were significantly upregulated in *lck*:RFP$^+$ cells from zT_{reg} cell-depleted damaged spinal cords (Figure S5P). Thus, inhibition of IFNγ-secreting T cells in the spinal cord may contribute to zebrafish spinal cord regeneration.

Interleukin-10 (IL-10) is a T_{reg} cell-derived immunosuppressive cytokine that promotes tissue repair in mice. As predicted, zT_{reg} cells expressed *il10* (Figure 6H), and were the major source of this cytokine in damaged tissues (Figure S6A). We assessed *il10* function using a homozygous *il10*^{sa1423} mutant (*il10*$^{-/-}$), which harbors a premature stop codon in exon 1 (Zebrafish Mutation Project, Sanger Institute) and fails to upregulate *il10* expression in damaged tissues (Figure S6B). *il10*$^{-/-}$ mutants exhibited an inflammatory cytokine expression profile with elevated *nos2b* expression and a concomitant reduction in *marco* expression in injured tissues, suggesting that *il10* has a conserved immunomodulatory role in zT_{reg} cells (Figures S6C–S6E).

Despite enhanced inflammation in *il10*$^{-/-}$ mutants, precursor cell proliferation was unaffected during regeneration (Figures S6F–S6K), and the expression of regeneration factors was similar to that in WT control tissues (Figures S6L–S6N). These results demonstrate that the zT_{reg} cell-mediated regenerative response is distinct from well-characterized IL-10-dependent immunomodulatory functions. Combined with our observation that *il10* expression in zT_{reg} cells was not induced in an organ-specific manner (Figure 6H), we conclude that zT_{reg} cell-derived production of tissue-specific regeneration factors is distinct from their canonical immunosuppressive role.

Foxp3a Is Required for the Expression of Tissue-Specific Regeneration Factors

We recently established a Foxp3a-deficient zebrafish mutant, *foxp3a*^{vcc6} (*foxp3a*$^{-/-}$) (Figure 7A), which exhibited increased inflammation similar to FOXP3-deficient mice (*Foxp3*$^{-/-}$) (Sugimoto et al., 2017). However, in contrast to *Foxp3*$^{-/-}$ mice, *foxp3a*$^{-/-}$ fish were grossly normal until 60 dpf, and nearly 50% survived with a moderate growth retardation beyond 90 dpf (Sugimoto et al., 2017), permitting regeneration studies in *foxp3a*$^{-/-}$ fish. To further explore the regulation of regeneration factor expression, we performed regeneration experiments with young adult *foxp3a*$^{-/-}$ mutants and *foxp3a*$^{+/+}$ clutch-mate controls. Spinal cord, heart, and retinal regeneration were severely impaired in *foxp3a*$^{-/-}$ fish (Figures S7A–S7F). Defective regeneration was not due to impaired infiltration of zT_{reg} cells, as we observed normal or even increased numbers of *foxp3a*:RFP$^+$ cells in the damaged organs of *foxp3a*:*RFP*;*foxp3a*$^{-/-}$ fish (Figures 7B and S7G–S7I). *foxp3a*$^{-/-}$ fish exhibited significantly reduced *il10* expression in damaged organs (Figures S7J–S7L), accompanied by increased inflammatory gene expression (Figures S7M–S7O), which is consistent with the known regulation of *IL10* expression by FOXP3 in mice and the elevated inflammation detected in the injured tissues of *il10*$^{-/-}$ fish (Figures S6C–S6E).

However, in contrast with the normal regenerative responses observed in *il10*$^{-/-}$ fish (Figures S6F–S6N), *foxp3a*$^{-/-}$ fish demonstrated a significant reduction in neurogenesis (Figures 7C and 7F) and proliferation of cardiomyocytes (Figures 7D and 7G) and Müller glia (Figures 7E and 7H), with a concomitant reduction in the expression of the precursor cell growth factors (Figures 7I–7K). To determine whether the regulation of regeneration factors could explain the regenerative failure, we purified *foxp3a*:RFP$^+$ cells from damaged *foxp3a*$^{-/-}$ tissues. Strikingly, similar to the strong downregulation of *il10*, the expression levels of *ntf3*, *nrg1*, and *igf1* were undetectable in *foxp3a*$^{-/-}$ zT_{reg} cells, showing that Foxp3a is required for the induction of regeneration factors by zT_{reg} cells (Figures 7L–7N). In contrast, *areg* expression was maintained in *foxp3a*$^{-/-}$ zT_{reg} cells, highlighting the specificity of the Foxp3a-dependent regenerative response (Figures 7L–7N).

DISCUSSION

Recent studies have shown that mouse T_{reg} cells promote tissue renewal by directly stimulating cell differentiation and proliferation in regeneration-competent tissues (Ali et al., 2017; Arpaia et al., 2015; Burzyn et al., 2013; Castiglioni et al., 2015; Dombrowski et al., 2017; Kuswanto et al., 2016; Nosbaum et al., 2016). We significantly expand our understanding of T_{reg} cell-mediated regeneration by defining a critical role for zT_{reg} cell-derived organ-specific growth factors in zebrafish tissues whose counterparts do not regenerate in mammals. We further demonstrate that the pro-regenerative role of zT_{reg} cells is functionally distinct from known IL-10-mediated immunomodulatory roles.

In the mouse, CNS and heart tissue does not exhibit robust regeneration after injury despite the recruitment of an

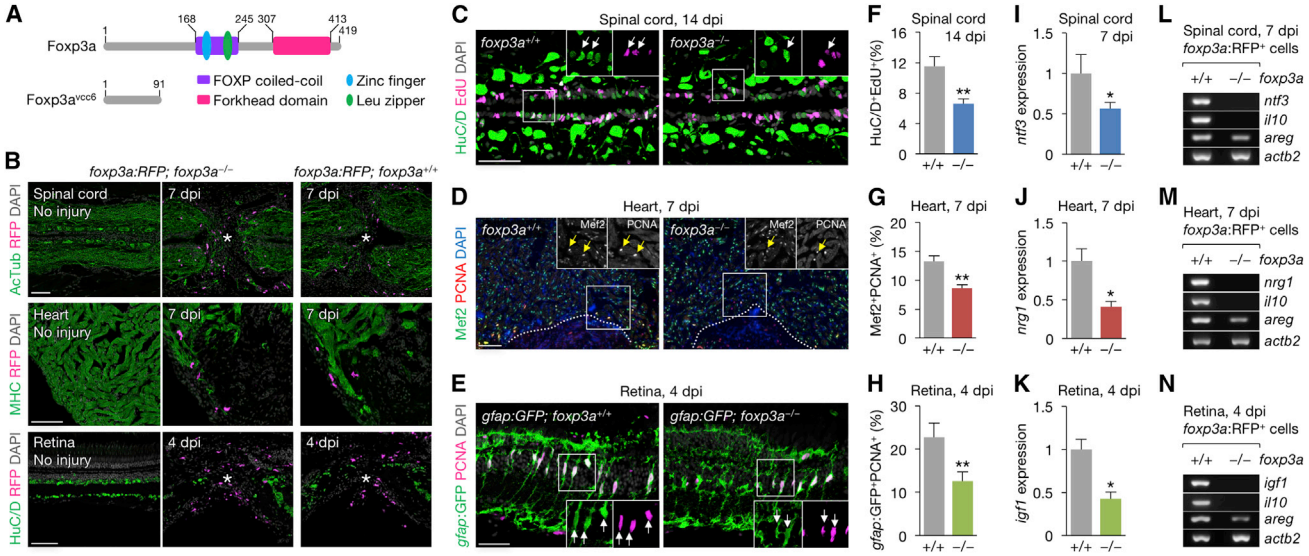

Figure 7. Impaired Regeneration in Foxp3a-Deficient Zebrafish

(A) Foxp3a domain structure and predicted truncated product of the *Foxp3a*^{vcc6} allele. Numbers indicate amino acid positions.

(B) Sections of Foxp3a-deficient (*foxp3a*$^{-/-}$) and WT (*foxp3a*$^{+/+}$) clutch-mate *foxp3a*:*RFP* fish. Asterisks indicate injury epicenter.

(C–E) Proliferation of newborn neurons (C), cardiomyocytes (D), and Müller glia (E). Insets show single-channel confocal slices (C and E) or epifluorescent images (D) of the demarcated regions. Arrows mark co-labeled cells. Dotted lines indicate the wound border.

(F–H) Quantification of (C), (D) and (E), respectively (mean ± SEM, n = 5–7).

(I–K) qRT-PCR analysis of regeneration factor genes (mean ± SEM, n = 6).

(L–N) Semi-qRT-PCR analysis of regeneration factor genes in purified *foxp3a*:RFP$^+$ cells. +/+, *foxp3a*$^{+/+}$; −/−, *foxp3a*$^{-/-}$.

Confocal projections of z stacks are shown, except for the epifluorescent images in (D). *p < 0.05, **p < 0.01, Mann-Whitney U test. Scale bars, 50 μm. See also Figure S7.

anti-inflammatory T_{reg} cell infiltrate that facilitates tissue repair (Kunis et al., 2015; Liesz et al., 2009; Raposo et al., 2014; Tang et al., 2012; Walsh et al., 2014; Weirather et al., 2014). The selective pressure to mount a rapid and strong inflammatory response to seal wounds with impermeable scars in terrestrial lineages may have limited mammalian T_{reg} cell pro-regenerative capacity (Aurora and Olson, 2014; Mescher and Neff, 2005). Alternatively, the intrinsic capacity to respond to T_{reg} cell stimulation in non-regenerative mammalian tissues may be limited postnatally (Porrello et al., 2011). Future studies will be needed to test whether manipulating mammalian T_{reg} cells to produce pro-regenerative factors, or increasing the sensitivity of the parenchymal cells to T_{reg} cell factors, or both are required to enhance regeneration in tissues that lack a robust regenerative response.

Our results suggest that the local injury environment instructs zT_{reg} cells to produce trophic and mitogenic factors that mediate the regeneration of destroyed cell types that are specific to the damaged tissue in which they reside. The mechanisms that mediate communication between zT_{reg} cells and the injury environment to activate tissue-specific regenerative programs remain unclear. Recently, macrophages have been shown to integrate local injury signals to activate tissue-specific repair functions (Bosurgi et al., 2017; Minutti et al., 2017), suggesting that interactions with macrophages could instruct the pro-regenerative functions of zT_{reg} cells. It will be important to address whether other tissue-resident immune cells or damaged parenchymal tissues might provide signals for the amplification or the recruitment of pro-regenerative zT_{reg} cells.

We found that Foxp3a is required for the induction of zT_{reg} cell-derived tissue-specific regenerative factors in injured tissues. Foxp3a may directly regulate pro-regenerative growth factors, since the human FOXP3 ortholog binds to *NRG1* and *IGF1* regulatory regions (Sadlon et al., 2010). Alternatively, Foxp3a may act as a co-transcription factor as described for the tissue-specific induction of a FOXP3-dependent transcriptional program in mouse visceral adipose tissue (VAT) T_{reg} cells (Cipolletta et al., 2012). VAT T_{reg} cells were defined by the high expression of PPARγ (peroxisome proliferator-activated receptor γ), a master regulatory transcription factor of fatty acid and glucose metabolism, which physically interacts with FOXP3 to regulate the expression fat metabolism genes. Similarly, spinal cord-, heart-, or retina-infiltrating zT_{reg} cells might be functionally distinguished by tissue-specific cofactors that refine the regenerative response. Additional *in vivo* data will be required to determine the mechanism by which Foxp3a activates the tissue-specific expression of Ntf3, Nrg1, and Igf1 in injury-associated zT_{reg} cells.

Although tissue regeneration is severely impaired in the absence of zT_{reg} cells, the residual expression of regeneration factors after zT_{reg} depletion and the *in situ* signal detected in parenchymal *foxp3a*:RFP$^-$ cells indicate that additional cell types also express these factors. Recent studies have identified perivascular cells as a source of Nrg1 in the heart (Gemberling et al., 2015) and Müller glia-derived progenitor cells as a source of Igf1 in the retina (Wan et al., 2014). These data suggest that successful regeneration requires multiple sources of precursor cell growth factors, and conditional ablation of each source will

be necessary to define the relative contribution of each cell type to precursor cell proliferation and regeneration.

This study demonstrates that organ regeneration is T_{reg} cell dependent, and identifies unique T_{reg} cell subsets that express distinct regeneration factor profiles. We propose that zT_{reg} cells retain a certain plasticity to support homeostasis and regeneration of diverse tissues by producing growth factors that specifically enhance regeneration of tissue-specific cell types. Given the remarkable capacity for zebrafish to regenerate multiple organs, investigating zT_{reg} cell function in additional regeneration contexts and elucidating the mechanism for pro-regenerative zT_{reg} cell differentiation may provide insights into how human T_{reg} cells can be precisely targeted to facilitate regeneration of damaged tissues.

STAR★METHODS

Detailed methods are provided in the online version of this paper and include the following:

- KEY RESOURCES TABLE
- CONTACT FOR REAGENT AND RESOURCE SHARING
- EXPERIMENTAL MODEL AND SUBJECT DETAILS
- METHOD DETAILS
  - Generation of Transgenic Animals
  - Injury Procedures
  - Axonal Tracing
  - Swim Path Tracking
  - Drug Administrations
  - Flow Cytometry and Cell Sorting
  - RT-PCR Analysis
  - Histological Assays
  - *In Situ* Hybridization
  - Microscopy
- QUANTIFICATION AND STATISTICAL ANALYSIS
  - Cell Number Quantification
  - Swim Path Measurement
  - Precursor Cell Proliferation Quantification
  - Apoptotic Cell Number Quantification
  - Quantification of Scar Size
  - Quantification of Myocardium Thickness
  - Statistical Analysis

SUPPLEMENTAL INFORMATION

Supplemental Information includes seven figures and one table and can be found with this article online at https://doi.org/10.1016/j.devcel.2017.11.010.

ACKNOWLEDGMENTS

We thank S. Malik, M. Nakayama, and D. Zhang for technical assistance; C. Jenkin, J. Martin, and K. Brennan for zebrafish care; E. Lam and R. Salomon for flow cytometry and FACS; K. Kawakami for plasmids; and R. Harvey, R. Graham, N. Rosenthal, S. Grey, S. Barry, J. Sprent, and C. Goodnow for discussions and comments on the manuscript. This work is supported by grants from NHMRC (APP1046469, APP1130247) and JDRF (T1DCRN Innovation Award).

AUTHOR CONTRIBUTIONS

Conceptualization, S.P.H. and K.K.; Methodology, D.Z.S., A.G.-R., and K.K.; Formal Analysis, D.H. and S.N.; Investigation, S.P.H., D.Z.S., K.S., A.G.-R., and K.K.; Writing – Original Draft, K.K.; Writing – Review & Editing, S.P.H., D.H., and K.K.; Supervision, K.K.; Project Administration, S.P.H. and K.K; Funding Acquisition, K.K.

Received: July 14, 2017
Revised: October 20, 2017
Accepted: November 13, 2017
Published: December 18, 2017

REFERENCES

Ali, N., Zirak, B., Rodriguez, R.S., Pauli, M.L., Truong, H.-A., Lai, K., Ahn, R., Corbin, K., Lowe, M.M., Scharschmidt, T.C., et al. (2017). Regulatory T cells in skin facilitate epithelial stem cell differentiation. Cell *169*, 1119–1129.

Andersen, K.G., Nissen, J.K., and Betz, A.G. (2012). Comparative genomics reveals key gain-of-function events in Foxp3 during regulatory T cell evolution. Front. Immunol. *3*, 113.

Arpaia, N., Green, J.A., Moltedo, B., Arvey, A., Hemmers, S., Yuan, S., Treuting, P.M., and Rudensky, A.Y. (2015). A distinct function of regulatory T cells in tissue protection. Cell *162*, 1078–1089.

Aurora, A.B., and Olson, E.N. (2014). Immune modulation of stem cells and regeneration. Cell Stem Cell *15*, 14–25.

Barbosa, J.S., Sanchez-Gonzalez, R., Di Giaimo, R., Baumgart, E.V., Theis, F.J., Götz, M., and Ninkovic, J. (2015). Live imaging of adult neural stem cell behavior in the intact and injured zebrafish brain. Science *348*, 789–793.

Becker, T., Wullimann, M.F., and Becker, C.G. (1997). Axonal regrowth after spinal cord transection in adult zebrafish. J. Comp. Neurol. *377*, 577–595.

Bernardos, R.L., and Raymond, P.A. (2006). GFAP transgenic zebrafish. Gene Expr. Patterns *6*, 1007–1013.

Bersell, K., Arab, S., Haring, B., and Kühn, B. (2009). Neuregulin1/ErbB4 signaling induces cardiomyocyte proliferation and repair of heart injury. Cell *138*, 257–270.

Beyer, M., Thabet, Y., Müller, R.-U., Sadlon, T., Classen, S., Lahl, K., Basu, S., Zhou, X., Bailey-Bucktrout, S.L., Krebs, W., et al. (2011). Repression of the genome organizer SATB1 in regulatory T cells is required for suppressive function and inhibition of effector differentiation. Nat. Immunol. *12*, 898–907.

Bosurgi, L., Cao, Y.G., Cabeza-Cabrerizo, M., Tucci, A., Hughes, L.D., Kong, Y., Weinstein, J.S., Licona-Limon, P., Schmid, E.T., Pelorosso, F., et al. (2017). Macrophage function in tissue repair and remodeling requires IL-4 or IL-13 with apoptotic cells. Science *356*, 1072–1076.

Brunkow, M.E., Jeffery, E.W., Hjerrild, K.A., Paeper, B., Clark, L.B., Yasayko, S.A., Wilkinson, J.E., Galas, D., Ziegler, S.F., and Ramsdell, F. (2001). Disruption of a new forkhead/winged-helix protein, scurfin, results in the fatal lymphoproliferative disorder of the scurfy mouse. Nat. Genet. *27*, 68–73.

Burns, C.G., Milan, D.J., Grande, E.J., Rottbauer, W., MacRae, C.A., and Fishman, M.C. (2005). High-throughput assay for small molecules that modulate zebrafish embryonic heart rate. Nat. Chem. Biol. *1*, 263–264.

Burzyn, D., Kuswanto, W., Kolodin, D., Shadrach, J.L., Cerletti, M., Jang, Y., Sefik, E., Tan, T.G., Wagers, A.J., Benoist, C., et al. (2013). A special population of regulatory T cells potentiates muscle repair. Cell *155*, 1282–1295.

Castiglioni, A., Corna, G., Rigamonti, E., Basso, V., Vezzoli, M., Monno, A., Almada, A.E., Mondino, A., Wagers, A.J., Manfredi, A.A., et al. (2015). FOXP3^{+} T cells recruited to sites of sterile skeletal muscle injury regulate the fate of satellite cells and guide effective tissue regeneration. PLoS One *10*, e0128094.

Chablais, F., Veit, J., Rainer, G., and Jaźwińska, A. (2011). The zebrafish heart regenerates after cryoinjury-induced myocardial infarction. BMC Dev. Biol. *11*, 21.

Cipolletta, D., Feuerer, M., Li, A., Kamei, N., Lee, J., Shoelson, S.E., Benoist, C., and Mathis, D. (2012). PPAR-γ is a major driver of the accumulation and phenotype of adipose tissue Treg cells. Nature *486*, 549–553.

Curado, S., Anderson, R.M., Jungblut, B., Mumm, J., Schroeter, E., and Stainier, D.Y.R. (2007). Conditional targeted cell ablation in zebrafish: a new tool for regeneration studies. Dev. Dyn. *236*, 1025–1035.

D'Uva, G., Aharonov, A., Lauriola, M., Kain, D., Yahalom-Ronen, Y., Carvalho, S., Weisinger, K., Bassat, E., Rajchman, D., Yifa, O., et al. (2015). ERBB2 triggers mammalian heart regeneration by promoting cardiomyocyte dedifferentiation and proliferation. Nat. Cell Biol. *17*, 627–638.

de Preux Charles, A.-S., Bise, T., Baier, F., Marro, J., and Jaźwińska, A. (2016). Distinct effects of inflammation on preconditioning and regeneration of the adult zebrafish heart. Open Biol. *6*, 160102.

Dee, C.T., Nagaraju, R.T., Athanasiadis, E.I., Gray, C., Fernandez Del Ama, L., Johnston, S.A., Secombes, C.J., Cvejic, A., and Hurlstone, A.F.L. (2016). $CD4^-$ transgenic zebrafish reveal tissue-resident Th2- and regulatory T cell-like populations and diverse mononuclear phagocytes. J. Immunol. *197*, 3520–3530.

Delgado, A.C., Ferron, S.R., Vicente, D., Porlan, E., Perez-Villalba, A., Trujillo, C.M., D'Ocón, P., and Fariñas, I. (2014). Endothelial NT-3 delivered by vasculature and CSF promotes quiescence of subependymal neural stem cells through nitric oxide induction. Neuron *83*, 572–585.

Dombrowski, Y., O'Hagan, T., Dittmer, M., Penalva, R., Mayoral, S.R., Bankhead, P., Fleville, S., Eleftheriadis, G., Zhao, C., Naughton, M., et al. (2017). Regulatory T cells promote myelin regeneration in the central nervous system. Nat. Neurosci. *20*, 674–680.

Fang, Y., Gupta, V., Karra, R., Holdway, J.E., Kikuchi, K., and Poss, K.D. (2013). Translational profiling of cardiomyocytes identifies an early Jak1/Stat3 injury response required for zebrafish heart regeneration. Proc. Natl. Acad. Sci. USA *110*, 13416–13421.

Fausett, B.V., and Goldman, D. (2006). A role for alpha1 tubulin-expressing Müller glia in regeneration of the injured zebrafish retina. J. Neurosci. *26*, 6303–6313.

Fischer, A.J., and Reh, T.A. (2002). Exogenous growth factors stimulate the regeneration of ganglion cells in the chicken retina. Dev. Biol. *251*, 367–379.

Fontenot, J.D., Gavin, M.A., and Rudensky, A.Y. (2003). Foxp3 programs the development and function of $CD4^+CD25^+$ regulatory T cells. Nat. Immunol. *4*, 330–336.

Fontenot, J.D., Rasmussen, J.P., Williams, L.M., Dooley, J.L., Farr, A.G., and Rudensky, A.Y. (2005). Regulatory T cell lineage specification by the forkhead transcription factor foxp3. Immunity *22*, 329–341.

Fukazawa, T., Naora, Y., Kunieda, T., and Kubo, T. (2009). Suppression of the immune response potentiates tadpole tail regeneration during the refractory period. Development *136*, 2323–2327.

Gemberling, M., Karra, R., Dickson, A.L., and Poss, K.D. (2015). Nrg1 is an injury-induced cardiomyocyte mitogen for the endogenous heart regeneration program in zebrafish. Elife *4*, e05871.

Goldshmit, Y., Sztal, T.E., Jusuf, P.R., Hall, T.E., Nguyen-Chi, M., and Currie, P.D. (2012). Fgf-dependent glial cell bridges facilitate spinal cord regeneration in zebrafish. J. Neurosci. *32*, 7477–7492.

González-Rosa, J.M., Martín, V., Peralta, M., Torres, M., and Mercader, N. (2011). Extensive scar formation and regression during heart regeneration after cryoinjury in zebrafish. Development *138*, 1663–1674.

Hasegawa, T., Hall, C.J., Crosier, P.S., Abe, G., Kawakami, K., Kudo, A., and Kawakami, A. (2017). Transient inflammatory response mediated by interleukin-1β is required for proper regeneration in zebrafish fin fold. Elife *6*, e22716.

Hofmann, U., Beyersdorf, N., Weirather, J., Podolskaya, A., Bauersachs, J., Ertl, G., Kerkau, T., and Frantz, S. (2012). Activation of $CD4^+$ T lymphocytes improves wound healing and survival after experimental myocardial infarction in mice. Circulation *125*, 1652–1663.

Hori, S., Nomura, T., and Sakaguchi, S. (2003). Control of regulatory T cell development by the transcription factor Foxp3. Science *299*, 1057–1061.

Huang, W.C., Yang, C.C., Chen, I.H., Liu, Y.M., Chang, S.J., and Chuang, Y.J. (2013). Treatment of glucocorticoids inhibited early immune responses and impaired cardiac repair in adult zebrafish. PLoS One *8*, e66613.

Hui, S.P., Nag, T.C., and Ghosh, S. (2015). Characterization of proliferating neural progenitors after spinal cord injury in adult zebrafish. PLoS One *10*, e0143595.

Jopling, C., Sleep, E., Raya, M., Martí, M., Raya, A., and Izpisúa Belmonte, J.C. (2010). Zebrafish heart regeneration occurs by cardiomyocyte dedifferentiation and proliferation. Nature *464*, 606–609.

Josefowicz, S.Z., Lu, L.F., and Rudensky, A.Y. (2012). Regulatory T cells: mechanisms of differentiation and function. Annu. Rev. Immunol. *30*, 531–564.

Kikuchi, K., Holdway, J.E., Werdich, A.A., Anderson, R.M., Fang, Y., Egnaczyk, G.F., Evans, T., MacRae, C.A., Stainier, D.Y.R., and Poss, K.D. (2010). Primary contribution to zebrafish heart regeneration by $gata4^+$ cardiomyocytes. Nature *464*, 601–605.

Kroehne, V., Freudenreich, D., Hans, S., Kaslin, J., and Brand, M. (2011). Regeneration of the adult zebrafish brain from neurogenic radial glia-type progenitors. Development *138*, 4831–4841.

Kunis, G., Baruch, K., Miller, O., and Schwartz, M. (2015). Immunization with a myelin-derived antigen activates the brain's choroid plexus for recruitment of immunoregulatory cells to the CNS and attenuates disease progression in a mouse model of ALS. J. Neurosci. *35*, 6381–6393.

Kuswanto, W., Burzyn, D., Panduro, M., Wang, K.K., Jang, Y.C., Wagers, A.J., Benoist, C., and Mathis, D. (2016). Poor repair of skeletal muscle in aging mice reflects a defect in local, interleukin-33-dependent accumulation of regulatory T cells. Immunity *44*, 355–367.

Kyritsis, N., Kizil, C., Zocher, S., Kroehne, V., Kaslin, J., Freudenreich, D., Iltzsche, A., and Brand, M. (2012). Acute inflammation initiates the regenerative response in the adult zebrafish brain. Science *338*, 1353–1356.

Lai, S.-L., Marín-Juez, R., Moura, P.L., Kuenne, C., Lai, J.K.H., Tsedeke, A.T., Guenther, S., Looso, M., and Stainier, D.Y. (2017). Reciprocal analyses in zebrafish and medaka reveal that harnessing the immune response promotes cardiac regeneration. Elife *6*, e25605.

Langenau, D.M., Ferrando, A.A., Traver, D., Kutok, J.L., Hezel, J.-P.D., Kanki, J.P., Look, A.T., and Trede, N.S. (2004). In vivo tracking of T cell development, ablation, and engraftment in transgenic zebrafish. Proc. Natl. Acad. Sci. USA *101*, 7369–7374.

Li, L., Yan, B., Shi, Y.Q., Zhang, W.Q., and Wen, Z.L. (2012). Live imaging reveals differing roles of macrophages and neutrophils during zebrafish tail fin regeneration. J. Biol. Chem. *287*, 25353–25360.

Liesz, A., Suri-Payer, E., Veltkamp, C., Doerr, H., Sommer, C., Rivest, S., Giese, T., and Veltkamp, R. (2009). Regulatory T cells are key cerebroprotective immunomodulators in acute experimental stroke. Nat. Med. *15*, 192–199.

Mescher, A.L., and Neff, A.W. (2005). Regenerative capacity and the developing immune system. Adv. Biochem. Eng. Biotechnol. *93*, 39–66.

Minutti, C.M., Jackson-Jones, L.H., García-Fojeda, B., Knipper, J.A., Sutherland, T.E., Logan, N., Rinqvist, E., Guillamat-Prats, R., Ferenbach, D.A., Artigas, A., et al. (2017). Local amplifiers of IL-4Rα-mediated macrophage activation promote repair in lung and liver. Science *356*, 1076–1080.

Mitra, S., Alnabulsi, A., Secombes, C.J., and Bird, S. (2010). Identification and characterization of the transcription factors involved in T-cell development, t-bet, stat6 and foxp3, within the zebrafish, *Danio rerio*. FEBS J. *277*, 128–147.

Moran, A.E., Holzapfel, K.L., Xing, Y., Cunningham, N.R., Maltzman, J.S., Punt, J., and Hogquist, K.A. (2011). T cell receptor signal strength in Treg and iNKT cell development demonstrated by a novel fluorescent reporter mouse. J. Exp. Med. *208*, 1279–1289.

Nosbaum, A., Prevel, N., Truong, H.A., Mehta, P., Ettinger, M., Scharschmidt, T.C., Ali, N.H., Pauli, M.L., Abbas, A.K., and Rosenblum, M.D. (2016). Cutting edge: regulatory T cells facilitate cutaneous wound healing. J. Immunol. *196*, 2010–2014.

Petrie, T.A., Strand, N.S., Yang, C.T., Rabinowitz, J.S., and Moon, R.T. (2015). Macrophages modulate adult zebrafish tail fin regeneration. Development *142*, 406.

Pisharath, H., Rhee, J.M., Swanson, M.A., Leach, S.D., and Parsons, M.J. (2007). Targeted ablation of beta cells in the embryonic zebrafish pancreas using *E. coli* nitroreductase. Mech. Dev. *124*, 218–229.

Polizzotti, B.D., Ganapathy, B., Walsh, S., Choudhury, S., Ammanamanchi, N., Bennett, D.G., dos Remedios, C.G., Haubner, B.J., Penninger, J.M., and Kühn, B. (2015). Neuregulin stimulation of cardiomyocyte regeneration in mice and

human myocardium reveals a therapeutic window. Sci. Transl. Med. *7*, 281ra45.

Porrello, E.R., Mahmoud, A.I., Simpson, E., Hill, J.A., Richardson, J.A., Olson, E.N., and Sadek, H.A. (2011). Transient regenerative potential of the neonatal mouse heart. Science *331*, 1078–1080.

Poss, K.D., Wilson, L.G., and Keating, M.T. (2002). Heart regeneration in zebrafish. Science *298*, 2188–2190.

Quintana, F.J., Iglesias, A.H., Farez, M.F., Caccamo, M., Burns, E.J., Kassam, N., Oukka, M., and Weiner, H.L. (2010). Adaptive autoimmunity and Foxp3-based immunoregulation in zebrafish. PLoS One *5*, e9478.

Raposo, C., Graubardt, N., Cohen, M., Eitan, C., London, A., Berkutzki, T., and Schwartz, M. (2014). CNS repair requires both effector and regulatory T cells with distinct temporal and spatial profiles. J. Neurosci. *34*, 10141–10155.

Reimer, M.M., Sörensen, I., Kuscha, V., Frank, R.E., Liu, C., Becker, C.G., and Becker, T. (2008). Motor neuron regeneration in adult zebrafish. J. Neurosci. *28*, 8510–8516.

Ritchey, E.R., Zelinka, C.P., Tang, J., Liu, J., and Fischer, A.J. (2012). The combination of IGF1 and FGF2 and the induction of excessive ocular growth and extreme myopia. Exp. Eye Res. *99*, 1–16.

Sadlon, T.J., Wilkinson, B.G., Pederson, S., Brown, C.Y., Bresatz, S., Gargett, T., Melville, E.L., Peng, K., D'Andrea, R.J., Glonek, G.G., et al. (2010). Genome-wide identification of human FOXP3 target genes in natural regulatory T cells. J. Immunol. *185*, 1071–1081.

Sakaguchi, S. (2004). Naturally arising $CD4^+$ regulatory t cells for immunologic self-tolerance and negative control of immune responses. Annu. Rev. Immunol. *22*, 531–562.

Sakaguchi, S., Miyara, M., Costantino, C.M., and Hafler, D.A. (2010). $FOXP3^+$ regulatory T cells in the human immune system. Nat. Rev. Immunol. *10*, 490–500.

Schindelin, J., Arganda-Carreras, I., Frise, E., Kaynig, V., Longair, M., Pietzsch, T., Preibisch, S., Rueden, C., Saalfeld, S., Schmid, B., et al. (2012). Fiji: an open-source platform for biological-image analysis. Nat. Methods *9*, 676–682.

Schnabel, K., Wu, C.C., Kurth, T., and Weidinger, G. (2011). Regeneration of cryoinjury induced necrotic heart lesions in zebrafish is associated with epicardial activation and cardiomyocyte proliferation. PLoS One *6*, e18503.

Senut, M.C., Gulati-Leekha, A., and Goldman, D. (2004). An element in the alpha1-tubulin promoter is necessary for retinal expression during optic nerve regeneration but not after eye injury in the adult zebrafish. J. Neurosci. *24*, 7663–7673.

Shimazu, K., Zhao, M., Sakata, K., Akbarian, S., Bates, B., Jaenisch, R., and Lu, B. (2006). NT-3 facilitates hippocampal plasticity and learning and memory by regulating neurogenesis. Learn. Mem. *13*, 307–315.

Sugimoto, K., Hui, S.P., Sheng, D.Z., Nakayama, M., and Kikuchi, K. (2017). Zebrafish FOXP3 is required for the maintenance of immune tolerance. Dev. Comp. Immunol. *73*, 156–162.

Tang, T.T., Yuan, J., Zhu, Z.F., Zhang, W.C., Xiao, H., Xia, N., Yan, X.X., Nie, S.F., Liu, J., Zhou, S.F., et al. (2012). Regulatory T cells ameliorate cardiac remodeling after myocardial infarction. Basic Res. Cardiol. *107*, 232.

Thornton, A.M., Korty, P.E., Tran, D.Q., Wohlfert, E.A., Murray, P.E., Belkaid, Y., and Shevach, E.M. (2010). Expression of Helios, an Ikaros transcription factor family member, differentiates thymic-derived from peripherally induced $Foxp3^+$ T regulatory cells. J. Immunol. *184*, 3433–3441.

Thummel, R., Kassen, S.C., Montgomery, J.E., Enright, J.M., and Hyde, D.R. (2008). Inhibition of Müller glial cell division blocks regeneration of the light-damaged zebrafish retina. Dev. Neurobiol. *68*, 392–408.

Traver, D., Paw, B.H., Poss, K.D., Penberthy, W.T., Lin, S., and Zon, L.I. (2003). Transplantation and in vivo imaging of multilineage engraftment in zebrafish bloodless mutants. Nat. Immunol. *4*, 1238–1246.

Trede, N.S., Langenau, D.M., Traver, D., and Look, A.T. (2004). The use of zebrafish to understand immunity. Immunity *20*, 367–379.

Urasaki, A., Asakawa, K., and Kawakami, K. (2008). Efficient transposition of the Tol2 transposable element from a single-copy donor in zebrafish. Proc. Natl. Acad. Sci. USA *105*, 19827–19832.

Walsh, J.T., Zheng, J., Smirnov, I., Lorenz, U., Tung, K., and Kipnis, J. (2014). Regulatory T cells in central nervous system injury: a double-edged sword. J. Immunol. *193*, 5013–5022.

Wan, J., Zhao, X.F., Vojtek, A., and Goldman, D. (2014). Retinal injury, growth factors, and cytokines converge on β-catenin and pStat3 signaling to stimulate retina regeneration. Cell Rep. *9*, 285–297.

Weirather, J., Hofmann, U.D.W., Beyersdorf, N., Ramos, G.C., Vogel, B., Frey, A., Ertl, G., Kerkau, T., and Frantz, S. (2014). $Foxp3^+$ $CD4^+$ T cells improve healing after myocardial infarction by modulating monocyte/macrophage differentiation. Circ. Res. *115*, 55–67.

Weiss, J.M., Bilate, A.M., Gobert, M., Ding, Y., Curotto de Lafaille, M.A., Parkhurst, C.N., Xiong, H., Dolpady, J., Frey, A.B., Ruocco, M.G., et al. (2012). Neuropilin 1 is expressed on thymus-derived natural regulatory T cells, but not mucosa-generated induced $Foxp3^+$ T reg cells. J. Exp. Med. *209*, 1723–1742.

Yadav, M., Louvet, C., Davini, D., Gardner, J.M., Martinez-Llordella, M., Bailey-Bucktrout, S., Anthony, B.A., Sverdrup, F.M., Head, R., Kuster, D.J., et al. (2012). Neuropilin-1 distinguishes natural and inducible regulatory T cells among regulatory T cell subsets in vivo. J. Exp. Med. *209*, 1713–1722.

STAR★METHODS

KEY RESOURCES TABLE

REAGENT or RESOURCE	SOURCE	IDENTIFIER
Antibodies		
Mouse monoclonal anti-acetylated tubulin	Sigma-Aldrich	Cat# T6793; RRID: AB_477585
Rabbit polyclonal anti-Caspase-3	Abcam	Cat# ab13847; RRID: AB_443014
Chicken polyclonal anti-GFP	Abcam	Cat# ab13970; RRID: AB_300798
Mouse monoclonal anti-HuC/HuD (16A11)	Thermo Fisher Scientific	Cat# A-21271; RRID: AB_221448
Rabbit polyclonal anti-Mef2 (C-21)	Santa Cruz Biotechnology	Cat# sc-313; RRID: AB_631920
Mouse monoclonal anti-myosin heavy chain (MHC)	Developmental Studies Hybridoma Bank	Cat# F59; RRID: AB_528373
Mouse monoclonal anti-PCNA	Sigma-Aldrich	Cat# P8825; RRID: AB_477413
Rabbit polyclonal anti-PCNA	Santa Cruz Biotechnology	Cat# sc-7907; RRID: AB_2160375
Rabbit polyclonal anti-SOX2	Abcam	Cat# Ab97959; RRID: AB_2341193
Rabbit polyclonal anti-tRFP	Evrogen	Cat# AB233; RRID: AB_2571743
Rabbit polyclonal anti-Tag(CGY)FP	Evrogen	Cat# AB121; RRID: AB_2716691
Goat anti-chicken Alexa Fluor 488, IgG (H+L)	Thermo Fisher Scientific	Cat# A-11039; RRID: AB_2534096
Donkey anti-rabbit Alexa Fluor 488, IgG (H+L)	Thermo Fisher Scientific	Cat# A-21206; RRID: AB_2535792
Donkey anti-mouse Alexa Fluor 488, IgG (H+L)	Thermo Fisher Scientific	Cat# A-21202; RRID: AB_141607
Donkey anti-rabbit Alexa Fluor 555, IgG (H+L)	Thermo Fisher Scientific	Cat# A-31572; RRID: AB_162543
Donkey anti-mouse Alexa Fluor 555, IgG (H+L)	Thermo Fisher Scientific	Cat# A-31570; RRID: AB_2536180
Cy5 AffiniPure Donkey Anti-Mouse IgG (H+L)	Jackson Immuno Research	Cat# 715-175-150; RRID: AB_2340819
Chemicals, Peptides, and Recombinant Proteins		
Tissue Freezing Medium	Leica Biosystems	Cat# 14020108926
DAPI (4',6- diamidino-2-phenylindole dihydrochloride)	Sigma-Aldrich	Cat# D9542
TRIzol Reagent	Thermo Fisher Scientific	Cat# 15596026
Recombinant human NT3/NTF3	PeproTech	Cat# 450-03
Recombinant human NRG1	R&D Systems	Cat# 5898-NR-050
Recombinant human IGF-1	R&D Systems	Cat# 291-G1
Fluoro-Ruby (tetra-methyl rhodamine dextran, 10,000 MW)	Thermo Fisher Scientific	Cat# D1817
Metronidazole	Sigma-Aldrich	Cat# M1547
Dimethyl Sulfoxide (DMSO)	Sigma-Aldrich	Cat# D4540
Fetal Bovine Serum	Thermo Fisher Scientific	Cat# 10082139
Newborn Calf Serum	Thermo Fisher Scientific	Cat# 26010066
Collagenase, type 2	Worthington Biochemical	Cat# LS004176
ACK lysing buffer	Thermo Fisher Scientific	Cat# A1049201
PrimeSTAR GXL DNA Polymerase	Takara Bio	Cat# R050A
Critical Commercial Assays		
Click-iT EdU Alexa Fluor 555 Imaging Kit	Thermo Fisher Scientific	Cat# C10338
Click-iT EdU Alexa Fluor 647 Imaging Kit	Thermo Fisher Scientific	Cat# C10340
Quick & Easy BAC Modification Kit	Gene Bridges	Cat# K001
BACMAX DNA Purification Kit	Epicentre	Cat# BMAX044
mMESSAGE mMACHINE Transcription SP6 Kit	Life Technologies	Cat# AM1340
Transcriptor First Strand cDNA Synthesis Kit	Roche	Cat# 04379012001
SensiFAST cDNA Synthesis Kit	BIOLINE	Cat# BIO-65053
GoTaq Green Master Mix	Promega	Cat# M7123

(*Continued on next page*)

Continued

REAGENT or RESOURCE	SOURCE	IDENTIFIER
SYBR Select Master Mix	Thermo Fisher Scientific	Cat# 4472908
RNAscope 2.5 HD Detection Reagent - RED	Advanced Cell Diagnostics	Cat# 322360
Experimental Models: Organisms/Strains		
Zebrafish: *Tg(cmlc2:EGFP)*^{f1}	Burns et al., 2005	*f1*
Zebrafish: *Tg(gfap:EGFP)*^{mi2001}	Zebrafish International Resource Center (ZIRC)	*mi2001*
Zebrafish: *il10*^{sa1423}	Zebrafis International Resource Center (ZIRC)	*sa1423*
Zebrafish: *TgBAC(foxp3a:TagRFP)*^{vcc3}	This paper	*vcc3*
Zebrafish: *TgBAC(lck:EGFP)*^{vcc4}	Sugimoto et al., 2017	*vcc4*
Zebrafish: *TgBAC(foxp3a:TagCFP-NTR)*^{vcc5}	This paper	*vcc5*
Zebrafish: *foxp3a*^{vcc6}	Sugimoto et al., 2017	*vcc6*
Zebrafish: *TgBAC(foxp3a:EGFP)*^{vcc10}	This paper	*vcc10*
Zebrafish: *TgBAC(lck:TagRFP)*^{vcc11}	This paper	*vcc11*
Oligonucleotides		
il10-scr-F: CATTTTACATTTAACAACATACATTTGAATTC ATTTGTC	This paper	N/A
il10-scr-R: GGAAAGCCCTCCACAAATGAGCAACAGTCA GTTTTGAATT	This paper	N/A
Primers for RT-PCR, see Table S1	This paper	N/A
RNAscope Probe -Dr-ntf3	Advanced Cell Diagnostics	428691
RNAscope Probe -Dr-nrg1	Advanced Cell Diagnostics	414131
RNAscope Probe -Dr-igf1	Advanced Cell Diagnostics	489251
Recombinant DNA		
BAC clone CH211-167B20	BACPAC Resources Center	http://bacpacresources.org/home.htm
BAC clone CH211-230I4	BACPAC Resources Center	http://bacpacresources.org/home.htm
Software and Algorithms		
Fiji (ImageJ)	Schindelin et al., 2012.	https://fiji.sc/
Flowjo	FlowJo, LLC	https://www.flowjo.com/
EthoVision XT	Noldus	http://www.nolduszebrafish.com/

CONTACT FOR REAGENT AND RESOURCE SHARING

For further information and requests for resources and reagents used in this study should be directed to and will be fulfilled by the Lead Contact, Kazu Kikuchi (K.Kikuchi@victorchang.edu.au).

EXPERIMENTAL MODEL AND SUBJECT DETAILS

Wild-type and genetically modified zebrafish of outbred Ekkwill (EK) or EK/AB mixed background strain ranging in age from 3 to 12 months were used in this study at approximately equal sex ratios. All transgenic strains were analyzed as hemizygotes. Details of the generation of new transgenic strains are described below. The zebrafish carrying the *il10*^{sa1423} allele was provided by the Zebrafish International Resource Center (ZIRC; Eugene, OR, USA). Genotyping was performed using a PCR restriction fragment length polymorphism method using il10-scr-F and il10-scr-R primers (Key Resources Table). *il10*^{sa1423} mutant zebrafish develop normally and are fertile, and we did not detect gross abnormalities in uninjured animals. The *foxp3a*^{vcc6} (Sugimoto et al., 2017), *TgBAC(lck:EGFP)*^{vcc4} (Sugimoto et al., 2017), *Tg(gfap:EGFP)*^{mi2001} (Bernardos and Raymond, 2006), and *Tg(cmlc2:EGFP)*^{f1} (Burns et al., 2005) were previously described. Fish were housed at approximately 5 fish per liter in custom made aquarium racks and fed three times daily. Water temperature was maintained at 28°C. All zebrafish husbandry and experiments were performed in accordance with institutional and national animal ethics guidelines and approved by Garvan Institute of Medical Research/St Vincent's Hospital Animal Ethics Committee.

METHOD DETAILS

Generation of Transgenic Animals

All transgenic constructs were generated by modifying BAC DNA using Red/ET recombineering (GeneBridges, Heidelberg, Germany) and purified for injections using the BACMAX DNA Purification kit (Epicentre, Madison, WI, USA). The *TgBAC*(*foxp3a*:*TagRFP*)^{vcc3} construct was generated by by inserting the TagRFP expression cassette into the CH211-167B20 BAC after the *foxp3a* translational start codon. The *TgBAC*(*foxp3a*:*EGFP*)^{vcc10} and *TgBAC*(*foxp3a*:*TagCFP-NTR*)^{vcc5} constructs were generated similarly. The final constructs were purified and co-injected into single cell-stage zebrafish embryos along with *tol2* transposase mRNA (Urasaki et al., 2008), which was transcribed from linearized pCS-TP plasmid using the mMESSAGE mMACHINE SP6 kit (Life Technologies, Carlsbad, CA, USA). The *TgBAC*(*lck*:*TagRFP*)^{vcc11} construct was generated by inserting the TagRFP expression cassette into the CH211-230I4 BAC after the *lck* translational start codon. The final construct was purified, linearized with *Sfi*I, and injected into single cell-stage embryos.

Injury Procedures

Spinal cord injury was performed on zebrafish anesthetized in Tricaine as described (Becker et al., 1997). Iridectomy scissors were used to make an incision through the skin at approximately 3.5 mm rostral to the anterior border of the dorsal fin. The spinal cord was exposed and completely transected with scissors. A kimwipe was used to blot the blood, and animals were revived in aquarium water. Sham injury was performed for swimming behavior analysis as described above without spinal cord transection.

Heart cryoinjury was performed on zebrafish anesthetized in Tricaine as described (Chablais et al., 2011; González-Rosa et al., 2011; Schnabel et al., 2011). Iridectomy scissors were used to make an incision through the skin and the pericardial sac, and the ventricular apex was exposed. A copper filament, which is 0.22 mm of diameter, was precooled in liquid nitrogen, and the tip of the filament was placed in contact with the apex for approximately 25 seconds, and released from the ventricle by applying approximately 10 μl of aquarium water, and animals were revived in aquarium water.

Retinal injury was performed on zebrafish anesthetized in Tricaine as described (Senut et al., 2004). Fine forceps were used to apply a slight ventral rotation of the eyeball to expose the sclera. The exposed sclera was stabbed four times with a 19G beveled needle; the needle was inserted to the length of the bevel and rotated approximately 90 degrees in each injury. A kimwipe was used to blot the blood, and animals were revived in aquarium water.

Axonal Tracing

Iridectomy scissors were used to make an incision through the skin at approximately 3–4 mm caudal to the spinal cord transection site. The spinal cord was exposed, and dry crystals of 1 μl of Fluoro-Ruby (tetra-methyl rhodamine dextran, 10,000 MW; Thermo Fisher Scientific, Waltham, MA, USA) were placed on the surface of the exposed cord. The incision was closed, and the spinal cord was collected 24 hours after the dye insertion for histological analysis.

Swim Path Tracking

Zebrafish were transferred to an opaque acrylic tank (length: 20 cm; width: 40 cm) containing aquarium water (depth: 8 cm) and acclimatized for 2 min. Zebrafish swimming was recorded for 10 min using a video camera (Panasonic HCV770M). Uninjured and sham-injured zebrafish were used as controls.

Drug Administrations

For zT_{reg} cell ablation experiments, *foxp3a*:*NTR* fish were placed in a small beaker of aquarium water containing 0.2% dimethyl sulphoxide (DMSO) and 15 mM freshly dissolved Mtz (M1547; Sigma, St. Louis, MO, USA). Fish were maintained in the dark and in this media for 10–12 hours (overnight), rinsed with fresh aquarium water, and returned to a recirculating aquatic system. For regeneration experiments, this treatment cycle was repeated for three consecutive days and continued every other day (Figure S1E). Aquarium water was changed daily and fresh Mtz was added each day. Recombinant human NT3/NTF3 (450-03; PeproTech, Rocky Hill, NJ, USA), recombinant human NRG1 (5898-NR-050; R&D Systems, Minneapolis, MN, USA) were reconstituted in PBS and injected intraperitoneally into *foxp3a*:*NTR* fish at a dose of 8.0 μg/g body weight. Recombinant human IGF-1 (291-G1; R&D Systems, Minneapolis, MN, USA) was reconstituted in PBS, and was intravitreally injected using a hamilton syringe (Hamilton robotics, NV, USA) through the front side of the eye at a dose of 1.0 μg/g body weight. For the cell proliferation assay, adult zebrafish were intraperitoneally injected with 50 μl of 10 mM EdU once daily at 4, 5, and 6 days after spinal cord and heart injuries and at 3 days after retina injury.

Flow Cytometry and Cell Sorting

To prepare kidney, spinal cord, and retina cell suspensions, tissues were dissected in ice-cold 0.9× PBS with 5% fetal bovine serum (staining buffer) and pushed through a cell strainer (40 μm; Falcon 2340) with a syringe plunger. Peripheral blood was obtained by puncturing the heart or dorsal aorta during analyses of cardiac cryoinjury. The collected blood was treated with ACK red blood cell lysing buffer (Thermo Fisher Scientific, Waltham, MA, USA) and suspended in ice-cold staining buffer. To prepare a cardiac cell suspension, the ventricle was dissected, placed into a microcentrifuge tube containing 0.9× PBS with 1 mg/ml collagenase type 2 (Worthington Biochemical, Lakewood, NJ, USA), and incubated for 40 min at room temperature with gentle pipetting every

10 min. Dissociated cells were washed and re-suspended in ice-cold staining buffer. The FACS analysis was performed on a LSRII SORP (BD Biosciences, San Jose, CA, USA), and cell sorting was performed on a FACSAria IIu (BD Biosciences). Data were analyzed using FlowJo software (Treestar, Ashland, OR, USA). Dead cells, defined as DAPI (4',6-diamidino-2-phenylindole) stained, and doublets were excluded from all analyses and sorting. Cells in the lymphoid fraction were sorted in two sequential steps and collected directly during the second sort into a microcentrifuge tube containing 1 ml of TRIzol reagent (Thermo Fisher Scientific, Waltham, MA, USA) for subsequent RT-PCR analysis.

RT-PCR Analysis

Total RNA was extracted using TRIzol reagent, and cDNA was subsequently synthesized either with the Transcriptor first strand cDNA synthesis kit (Roche, Basel, Switzerland) or SensiFAST cDNA Synthesis Kit (Bioline, Australia). qRT-PCR was performed using a LightCycler 480 system (Roche, Basel, Switzerland). For semi-qRT-PCR, genes of interest were amplified using a PrimeSTAR GXL kit (Clontech, Palo Alto, CA, USA). The amount of cDNA was normalized according to *actb2*/*β-actin2* amplification in qRT-PCR and semi-qRT-PCR experiments. All qRT-PCR were performed using SYBR™ Select Master Mix (Applied Biosystems, CA, USA) and results obtained from 3–5 biological replicates. For details of the primers used in RT-PCR analysis, see Table S1.

Histological Assays

Picro-Mallory and Luxol fast blue staining were performed using standard protocols, and immunofluorescence was performed in paraformaldehyde fixed 10 μm cryosections. The slides were rinsed twice in PBS + 1% Tween-20 (PBT) for 5 min each and followed by incubation in NCS-PBT (10% newborn calf serum, 1% DMSO, in PBT) for 60 min at 37°C and then incubation in primary antibody for overnight at 4°C. See the Key Resources Table for details on primary and secondary antibodies used for immunofluorescence.

In Situ Hybridization

In situ hybridization using RNAscope probes (Advanced Cell Diagnostics, Hayward, CA) was performed on spinal cord, heart and retina tissues fixed with 4% paraformaldehyde for 24 hours at 4°C and equilibrated in 30% sucrose for another 24 hours, embedded in Tissue freezing medium (TFM; Leica Biosystems, Wetzlar, Germany), and cryosectioned to 10 μm. Tissue sections were washed twice with PBS for 5 min to remove TFM, followed by incubation in hydrogen peroxide for 10 min at room temperature, boiling in target retrieval for 5 min. After target retrieval, slides were briefly washed with distilled water and incubated for 5 min at 40°C with Protease Plus. Following all pretreatments, the manufacturer's protocol for RNAscope 2.5 HD Detection Kit-Red (Advanced Cell Diagnostics) was followed to hybridize probes and detect the signals. Immunostaining using anti-tRFP (see Key Resources Table) was performed following detection of *ntf3*, *nrg1* and *igf1* mRNA signals in RNAscope and tissue sections were incubated with primary antibodies overnight at 4°C. The *ntf3*, *nrg1* and *igf1* RNA probes used in this study were designed and synthesized by Advanced Cell Diagnostics.

Microscopy

Picro-Mallory and Luxol fast blue stained heart tissue sections were imaged on a Leica DM4000 B microscope (Leica Camera AG, Wetzlar, Germany), and immunofluorescence sections were imaged using a Zeiss AXIO imager M1 microscope (Carl Zeiss AG, Oberkochen, Germany). Confocal images were taken with a Zeiss LSM 710 confocal microscope (Carl Zeiss AG).

QUANTIFICATION AND STATISTICAL ANALYSIS

Cell Number Quantification

zT_{reg} cells in regenerating organs were imaged in the damaged areas of the spinal cord (1388 × 278 pixels), heart (1388 × 145 pixels), and retina (1388 × 145 pixels) using a 10× objective (Carl Zeiss AG), and *foxp3a*:RFP$^+$ cells were manually counted using ImageJ software (US National Institutes of Health, Bethesda, MD, USA). *lck*:RFP$^+$ T cells were similarly quantified. The results from three selected sections were averaged to determine the number of RFP$^+$cells in each spinal cord, heart and retina.

Swim Path Measurement

Total distance of swim path was obtained from the video recording of swimming zebrafish using EthoVisionXT software (Noldus, Wageningen, The Netherlands). The data were represented as mean ± SEM. Student's *t*-test with Welch correction was used.

Precursor Cell Proliferation Quantification

To quantify neurogenesis, images of the wound site, including both the rostral and caudal stumps, were taken at 7 and 14 dpi (1388 × 278 pixels) by using a Zeiss AXIO imager M1 microscope (Carl Zeiss AG). The numbers of either Sox2$^+$ and Sox2$^+$PCNA$^+$ cells, or HuC/D$^+$ and HuC/D$^+$EdU$^+$ cells, were manually counted using ImageJ software. The percentages of Sox2$^+$PCNA$^+$ or HuC/D$^+$EdU$^+$ cells from three selected sections were averaged to determine the proliferation indices of neural progenitor cells and immature neurons in each spinal cord. To quantify cardiomyocyte proliferation, images of the injury border zone area were taken at 7 dpi (967 × 267 pixels), and the numbers of Mef2$^+$ and Mef2$^+$PCNA$^+$ cells were manually counted using ImageJ software. The percentages of Mef2$^+$PCNA$^+$ cells from three selected sections were averaged to determine the cardiomyocyte proliferation index in each heart. To quantify Müllar glia proliferation, images of the injury border zone area were taken at 4 dpi (967 × 145 pixels), and the

numbers of *gfap*:GFP$^+$ and *gfap*:GFP$^+$PCNA$^+$ cells were manually counted using ImageJ software. The percentages of *gfap*:GFP$^+$ PCNA$^+$ cells from three selected sections were averaged to determine the Müllar glia proliferation index in each retina.

Apoptotic Cell Number Quantification

Apoptotic cells in injured spinal cords, hearts, and retinas were detected by immunostaining with active Caspase-3 antibody (see Key Resources Table). Neurons and cardiomyocytes and Müllar glia undergoing apoptosis were imaged and quantified similarly as described in previous section, except that the numbers of HuC/D$^+$ and HuC/D$^+$Caspase-3$^+$ cells, myosin heavy chain MHC$^+$ and MHC$^+$Caspase-3$^+$, *gfap*:GFP$^+$ and *gfap*:GFP$^+$Caspase-3$^+$ cells were counted in injured spinal cords, hearts, and retinas.

Quantification of Scar Size

To quantify the scar tissue size in total ventricular area, one set of three serial sections of the 45 dpi whole heart were stained and images of all stained sections with the scar site were taken with a 5× objective (2048 × 1536 pixels). The size of the scar area (blue collagen and orange-red fibrin stained) and whole ventricular area were manually measured using ImageJ software. The percentages of scar area in respect to total ventricular area were averaged to determine the scar size.

Quantification of Myocardium Thickness

To quantify the thickness of myocardial wall surrounding the scar tissue, the distances between the apex and the approximate apical border of the scar tissue region were measured using ImageJ software. The results from three selected sections were averaged to determine the thickness of the myocardial wall surrounding the scar tissue.

Statistical Analysis

All statistical values are represented as mean ± SD or mean ± SEM. To determine the statistical significance, the *P* values were calculated either with Mann–Whitney *U* tests, Student's *t*-tests, Fisher's exact tests and *P* values less than 0.05 considered as statistically significant. All qRT-PCR results were obtained from 3–5 biological replicates. Statistical methods, sample size and *P* values are also described in the figure legends.